Scale-Dependent Transition in Soil Moisture Memory and Its Environmental Controls in Complex Mountain Terrain

Jun Zhang[1,2,3], Songtang He[1*], Yong Li[1], Yuan Xue[2]

[1] Key Laboratory of Mountain Hazards and Engineering Resilience /Institute of Mountain Hazards and Environment, Chinese Academy of Sciences, Chengdu 610041, China

[2] State Key Laboratory of Hydroscience and Engineering; Department of Hydraulic Engineering, Tsinghua University, Beijing 100084, China

[3] University of Chinese Academy of Sciences, Beijing 100049, China

Correspondence: Songtang He (hest@imde.ac.cn)

Abstract: Soil moisture memory (SMM) – the persistence of soil moisture anomalies – is a key factor preconditioning hydrological responses and geohazard susceptibility. ~~defines the antecedent wetness states that modulate catchment responses to meteorological triggers, serving as a critical determinant of background hydraulic susceptibility~~. However, how SMM varies across timescales and what controls its persistence in complex terrain remain poorly understood. ~~its multi-scale characteristics and environmental drivers remain poorly understood in complex terrain.~~ Here, we quantify~~This study characterizes~~ SMM dynamics across daily-to-interannual scales using 20-year (2003–2022) daily soil moisture data from three contrasting watersheds in southwestern China, prone to soil erosion (Dali River Basin), shallow landslides (Anning River Basin), and debris flows (Jiangjia Ravine). Integrating Power Spectrum Analysis (persistence strength), Detrended Fluctuation Analysis (DFA-2; persistence duration), and scale-dependent attribution via Boruta random forest with partial correlation, we identify a pronounced scale-dependent transition in SMM and its drivers.~~daily data (2003–2022) from three hazard-prone watersheds in southwestern China (Dali River, Anning River, and Jiangjia Ravine). By integrating Power Spectrum Analysis,~~

~~Detrended Fluctuation Analysis (DFA-2), and a spatial attribution modeling framework, we identify a distinct scale-dependent transition in SMM persistence and its controls.~~ ~~Results revealed that while~~ SMM~~memory~~ intensity generally weakened with increasing timescale, yet humid catchments exhibit surprisingly strong and persistent memory extending to multi-year scales.~~exhibited a robust "inherent persistence" regime extending to multi-year scales~~. Feature importance analysis reveals a critical structural shift around~~Crucially, feature importance analysis uncovered a structural transition at approximately~~ the 5-year scale: short-term memory is dominated by atmospheric forcing and vegetation, whereas long-term persistence is controlled by~~atmospheric variables and vegetation dominated short-term variability, whereas~~ soil properties and topography~~ governed the system's long-term~~. This transition marks a conceptual shift from event-driven fast-response (topography-mediated) to storage-dominated slow-response (soil-buffered) regimes.~~capacity to integrate low-frequency signals. Mechanistically, this marks a shift from event-driven hydraulic responses to background storage trends regulated by deep soil buffering.~~ These findings provide a framework~~basis~~ for distinguishing short-term~~event-scale~~ hydraulic preconditioning from long-term background susceptibility, proposing~~offering~~ a conceptual framework for incorporating~~a conceptual framework for incorporating~~ memory timescales ~~operational persistence horizons~~ into multi-scale geohazard assessment~~hierarchical hazard assessment strategies~~.

Keywords: Soil moisture memory; Driving Factor; Persistence horizon; Power spectrum analysis; Detrended fluctuation analysis

1. Introduction

Soil moisture memory (SMM) is a ~~critical~~ key driver of mountain hazards~~, including~~ such as debris flows, landslides, and soil erosion (An et al., 2025; Hu et al., 2015; Moragoda et al., 2022). ~~Mechanistically, e~~Elevated antecedent soil moisture increases pore water pressure, reduces effective stress and shear strength, ~~by increasing pore water pressure,~~ and thereby lowers the critical threshold for slope failure~~predisposing slopes to instability~~. While intense precipitation serves~~acts~~ as the direct~~immediate~~ trigger, antecedent ~~soil~~ moisture conditions determine the system~~landscape~~'s proximity to instability and precondition slope susceptibility~~susceptibility by determining how close the system is to its critical failure thresholds~~ (Bogaard et al., 2018; Cai et al., 2019). ~~Beyond this immediate mechanical role, t~~The persistence of SMM~~,~~ quantified by its memory timescale (t_{SMM})~~length, theoretically~~ defines the timescale over which antecedent signals influence hydraulic preconditioning, offering critical information~~persist, providing essential information on hydraulic preconditioning~~ for early warning systems (Bogaard et al., 2016; Huang et al., 2022; Wicki et al., 2020).

Soil moisture memory (SMM) ranges from days to years and is controlled by various factors (e.g., atmospheric forcing, soil properties, vegetation, and topography) (Entin et al., 2000; McColl et al., 2017; Rahmati et al., 2024). In mountain catchments, the pronounced spatial heterogeneity of these factors increases the sensitivity of hazard initiation to antecedent moisture while shortening hydrological response times (Bogaard & Greco, 2016; Dymond et al., 2021; Wicki et al., 2020). For instance, landslide probability increases exponentially once soil moisture exceeds critical thresholds of ~30–40 % (Mirus et al., 2018; Wicki et al., 2021), with slope angle acting as a key topographic modulator. For debris flows, antecedent soil moisture influences not only initiation probability, but

also runout distance (Coe et al., 2008). Similarly, soil loss rates under wet antecedent conditions can be 3–5 times higher than under dry conditions at equivalent rainfall intensities (Ran et al., 2012). Despite this established importance, systematic studies tracing SMM evolution across contiguous timescales—from monthly to seasonal, annual, and multi-year—remain scarce, particularly in steep mountain terrain (Entin et al., 2000; Nicolai-Shaw et al., 2016; Zhang et al., 2025). Additionally, unraveling the mechanisms behind SMM variation is challenging due to the complex interplay of topographic, pedological, meteorological, and vegetation controls (Brocca et al., 2007; Dong et al., 2018; Peng et al., 2023; Schönauer et al., 2024; Varga et al., 2020). Therefore, our study focuses on mountainous areas prone to natural hazards, aiming to quantify SMM variations and identify the dominant controlling factors across multiple timescales. ~~However, translating this theoretical memory into operational forecasts requires further validation against historical hazard events.~~

Furthermore, previous studies have explored driving factors of soil moisture variability at discrete temporal scales (Blanka-Végi et al., 2025; Cho et al., 2014; Fang et al., 2016; Kursa et al., 2010). For instance, Blanka-Végi et al. (2025) identified wilting point and evapotranspiration as key factors influencing SM at the annual scale using machine learning algorithms (MLR, SVR, XGBoost, and DNN). Similarly, other studies have demonstrated that vegetation type, soil texture, and precipitation also affect SMM (Brocca et al., 2012; Fang et al., 2016; Zhang et al., 2021, 2025). Nevertheless, the factors governing SMM across various temporal scales have received limited investigation, particularly in mountain areas. The mechanism that multi-scale SMM influence mountain hazard initiation and development remains largely unexplored.

~~Empirical evidence from various hazards supports this mechanistic understanding. Specifically, landslide probability increases exponentially when soil moisture (a proxy for pore-water pressure~~

~~saturation) exceeds a critical threshold of 30 ~ 40 % (Mirus et al., 2018; Wicki et al., 2021). While these studies define the critical state, quantifying the SMM persistence provides the essential temporal window required to estimate how long antecedent rainfall continues to drive the system toward this saturation threshold (Mirus et al., 2018). For debris flows, antecedent soil moisture conditions determine not only the likelihood of initiation but also the potential runout distance (Coe et al., 2008). Furthermore, under identical rainfall intensity, the soil loss rate can be 3 to 5 times higher under wet antecedent conditions than under dry conditions (Ran et al., 2012). Collectively, this evidence highlights the fundamental importance of quantifying SMM to understand how antecedent conditions modulate hazard initiation thresholds. Nonetheless, a comprehensive, multi-scale characterization of how SMM evolves from monthly to seasonal, annual, and multi-year scales remains limited (Entin et al., 2000; Nicolai-Shaw et al., 2016; Zhang et al., 2025). Unlike immediate meteorological triggers, this multi-scale memory reflects the system's inertia and defines the baseline hydrological state of the catchment in response to external forcing. However, elucidating its drivers is challenging due to the combined effects of diverse factors—topographic, pedological, meteorological, and vegetation (Brocca et al., 2007; Dong et al., 2018; Schönauer et al., 2024; Varga et al., 2020). Their strong interactions further complicate the disentanglement of individual and joint effects (Peng et al., 2023).~~

~~Previous studies have explored driving factors of soil moisture variability at discrete temporal scales (Blanka-Végi et al., 2025; Cho et al., 2014; Fang et al., 2016; Kursa et al., 2010), identifying, for instance, wilting point and evapotranspiration as key at the annual scale (Blanka-Végi et al., 2025) or vegetation type at the monthly scale (Fang et al., 2016). However, by focusing on individual scales, these studies have seldom established a systematic hierarchy of the relative~~

~~importance between static and dynamic factors across continuous temporal scales. This lack of a unified, scale-explicit framework prevents a mechanistic understanding of SMM persistence and limits the development of hazard assessment models capable of distinguishing background hydraulic loading from immediate event triggering (Li et al., 2025; Zhang et al., 2024).~~

In this study, we selected three catchments—Dali River Basin, Anning River Basin, and Jiangjia Ravine (representing distinct hazard regimes) — to research SMM characteristics and their scale-dependent drivers. The Power Spectrum Analysis (PSA) was used to investigate SMM characteristics. Subsequently, we employed DFA-2 method to identify characteristic persistence timescales. Moreover, to quantify the influence of environmental drivers, we employed scale-dependent attribution based on Boruta random forest combined with partial correlation analysis. Leveraging a two-decade daily soil moisture dataset, this study aims to: (1) quantify the scale-transition threshold and hierarchical drivers of SMM; (2) establish a quantitative hierarchy of driving factors across temporal scales; and (3) propose a conceptual framework that links multi-scale SMM to differentiated hazard preconditioning mechanisms, providing testable hypotheses for future event-based validation. ~~While previous studies have established the existence of soil moisture memory (SMM) and its general scale dependence at global or continental scales (e.g., Entin et al., 2000; Nicolai-Shaw et al., 2016), a critical gap persists in mechanistically linking this multi-scale memory to specific hydrological processes and practical hazard prediction within the complex terrain where these hazards predominantly occur. To bridge this gap, this study leverages a two-decade-long daily soil moisture dataset across three contrasting, hazard-prone watersheds with the following objectives: (1) to quantify the scale-transition threshold and hierarchical drivers of SMM; (2) to establish a quantitative hierarchy of driving factors across temporal scales; and (3) to develop~~

~~a conceptual framework linking multi-scale SMM to differentiated hazard preconditioning mechanisms. While direct validation against site-specific hazard inventories is beyond our current scope due to the spatial resolution mismatch (1-km pixels vs. slope-scale failures), we synthesize our findings with published hazard-SMM relationships (e.g., Mirus et al., 2018; Wei et al., 2025) to demonstrate the potential for SMM-informed early warning systems.~~ The paper is structured as follows: Section 2 describes the study areas, data, and methods. Section 3 presents the results~~,~~; Section 4 provides the discussion; and~~which are discussed in Section 4. Finally,~~ Section 5 summarizes~~provides~~ the main conclusions.

2. Materials and Methods

This study investigates soil moisture (SM) dynamics and their drivers across three hydro-climatically and geomorphologically distinct watersheds: the Dali River Basin, Anning River Basin, and Jiangjia Ravine. The Dali River Basin, located on the Loess Plateau, represents a semi-arid erosion-dominated system where soil moisture deficits and intense summer storms drive severe soil loss (Liu et al., 2023). The Anning River Basin and Jiangjia Ravine, located in southwestern China—a global hotspot for rainfall-triggered landslides and debris flows due to complex terrain, active tectonics, and intense monsoon precipitation (Wei et al., 2025; Yang et al., 2023)—represent humid landslide-prone and high-frequency debris flow environments, respectively. This gradient design spanning semi-arid to humid climates and erosion to mass-movement hazards enables identification of both commonalities and differences in SMM mechanisms across contrasting mountain environments. We incorporated static and dynamic variables—spanning topography, soil properties, meteorological conditions, and vegetation indices—from multiple authoritative datasets. SM temporal memory and persistence horizons were quantified using Power Spectral Analysis (PSA)

and second-order Detrended Fluctuation Analysis (DFA-2), respectively, while the Boruta–Random Forest algorithm was employed to quantify variable importance across spatial and temporal scales. The integrated use of these methods is designed to address complementary aspects of our research questions:

- Power Spectral Analysis (PSA) is used to characterize the overall distribution of SM variance across timescales (from daily to interannual), identifying the dominant frequencies of variability (Kantelhardt et al., 2006; Parada et al., 2003).
- Second-order Detrended Fluctuation Analysis (DFA-2) is specifically chosen to robustly quantify long-range persistence (memory) and to distinguish it from short-term correlations, providing a direct measure of the memory timescale (τ) (Kantelhardt et al., 2001; Zhang et al., 2025).
- The Boruta–Random Forest algorithm serves to identify and rank the key drivers (both static and dynamic) of SM memory across different temporal scales, handling high-dimensional data and complex, non-linear interactions without prior assumptions about variable relationships (Breiman, 2001; Kursa et al., 2010).

Together, this multi-method framework allows us to not only quantify how strong and how long SM memory persists, but also to attribute why it varies across scales and locations~~The overall research framework is illustrated in~~ (Fig. 1).

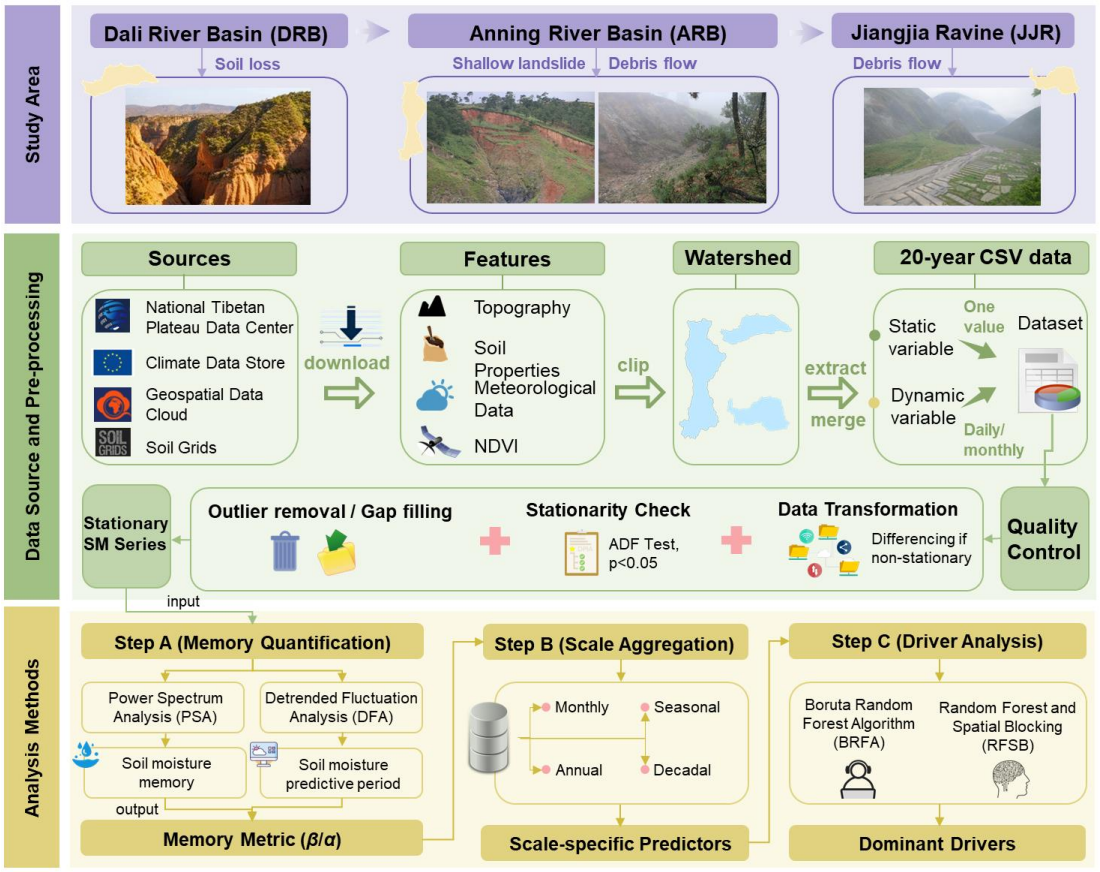

Fig. 1 Schematic workflow of the multi-scale soil moisture memory (SMM) analysis framework. The framework comprises three stages: (1) data preparation, where multi-source static (topography, soil) and dynamic (meteorology, vegetation) variables are harmonized and soil moisture time series undergo quality control and stationarity verification; (2) memory quantification, using Power Spectral Analysis (PSA) to characterize variance distribution across frequencies and Detrended Fluctuation Analysis (DFA-2) to derive memory timescales; and (3) driver attribution, applying the Boruta-Random Forest algorithm to identify scale-dependent importance of controlling factors. This integrated workflow resolves the strength, duration, and controls of SMM across timescales.~~Research framework of this study. The workflow integrates multi-source data processing, memory quantification, and driver identification. Key pre-processing steps include outlier removal and stationarity checks (ADF test) to ensure time stability. Soil moisture memory is quantified using Power Spectrum Analysis (PSA) and Detrended Fluctuation Analysis (DFA-2), followed by a multi-scale driver analysis using the Boruta algorithm across monthly to decadal aggregation windows.~~

The overall research framework is shown in Figure 1, outlining the data flow, analysis steps,

and their complementary roles in the multi-scale quantification and attribution of SMM.

2.1 Study Area

We selected three hydro-climatically distinct watersheds in southwestern China to represent a spectrum of mountain hazard environments (Fig. 2; detailed physiographic characteristics are provided in Appendix B and Table B1). These three basins were purposefully selected to cover a diverse range of hydro-climatic conditions (semi-arid to humid) and geomorphic types (loess plateau to steep tectonic valleys), allowing for a robust comparative analysis of SMM drivers across contrasting mountain terrains.

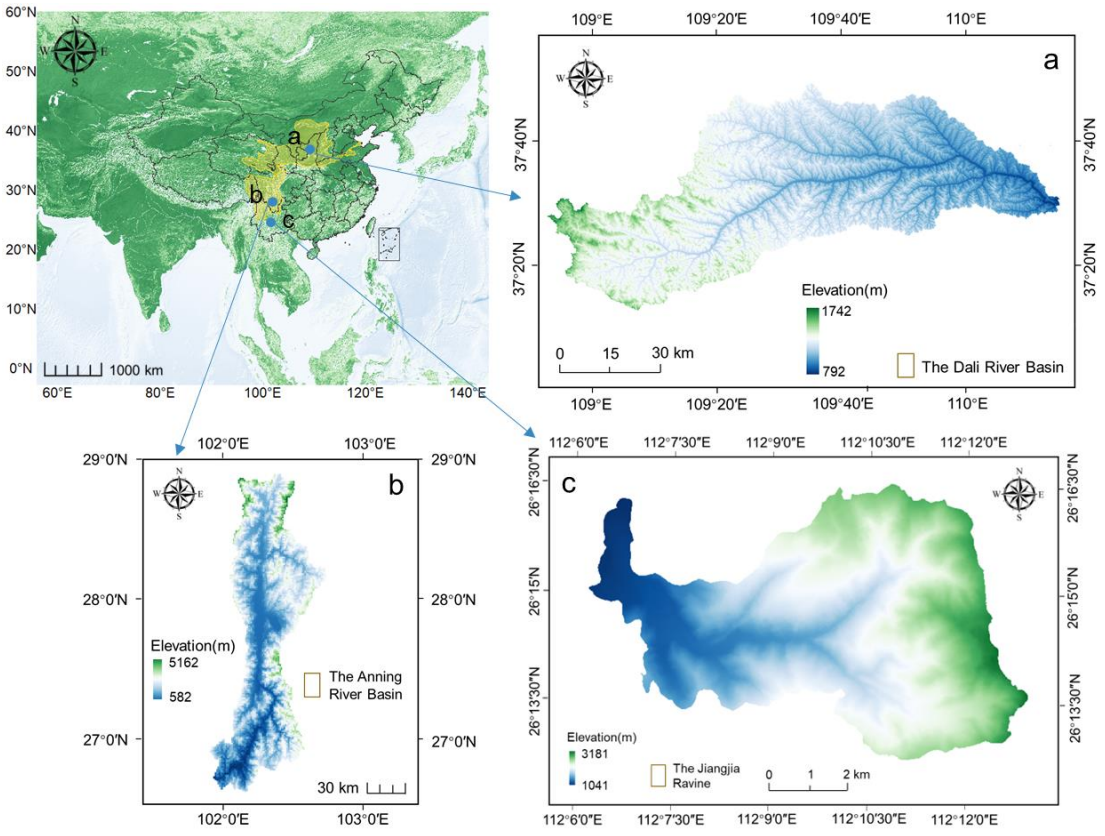

Fig. 2 Location of the study areas: (a) the Dali River Basin (DRB), (b) the Anning River Basin, (c) the Jiangjia Ravine.

- **Dali River Basin (DRB):** Semi-Arid Erosion-Prone System. Located on the Chinese

Loess Plateau (3,906 km^2), the DRB features steep loess terrain (avg. slope 17°) and highly erodible soils (silt > 60 %). The climate is semi-arid continental, with precipitation highly concentrated in summer storms (> 70 % from May to September), leading to persistent soil moisture deficits and severe erosion rates (Liu et al., 2020; Zhang et al., 2023).

- **Anning River Basin (ARB):** Complex Mountain-Valley System. Situated in southwestern Sichuan (11,150 km^2), the ARB is characterized by dramatic relief (900–4,750 m) and vertical climatic zonation. It operates under a humid subtropical-monsoon climate (~ 1,070 mm rainfall) with dense forest cover (Chen et al., 2024). Consequently, soil moisture dynamics are strongly regulated by vegetation phenology and the buffering capacity of deep forest soils (Yin et al., 2020).
- **Jiangjia Ravine (JJR):** Debris-Flow Dominated Catchment. A small (48.6 km^2) but extremely steep catchment in the Xiaojiang fault zone. Intense monsoon rainfall (> 85 % in May–Oct) combined with fractured geology drives rapid hydrological response cycles: rapid saturation during storms followed by quick drainage (Yang et al., 2023). This makes JJR a classic environment for high-frequency debris flows (Wei et al., 2025).
- Despite the large difference in basin area (ARB: 11,150 km² vs. JJR: 48.6 km²), a scale-matching sensitivity analysis (Appendix H) confirms that the observed differences in soil moisture memory between basins reflect intrinsic hydrological and landscape characteristics rather than artifacts of spatial averaging or domain size.

2.2 Data Sources and Preprocessing

We constructed a dataset comprising 12 static and dynamic covariates (Table 1) alongside daily

soil moisture (SM) data (1-km resolution) for ~~the period~~ 2003–2022. These covariates were selected based on an extensive literature review of soil moisture drivers (Rahmati et al., 2024; Seneviratne et al., 2010), prioritizing variables that are (1) widely recognized as key controls on SMM (topography, soil properties, meteorology, vegetation), (2) frequently used in prior multi-scale SMM studies, and (3) available at consistent spatial and temporal resolution with high reliability across the study region.

Soil Moisture Dataset: We utilized the all-weather 1-km daily soil moisture (SM) product developed by Song et al. (2022) ~~for the period 2003–2022~~. ~~Unlike raw reanalysis data or coarse passive microwave retrievals, t~~This dataset employs a machine learning-based spatiotemporal reconstruction framework to generate seamless high-resolution estimates by downscaling and fusing coarse-resolution passive microwave observations (AMSR-E/2) with high-resolution optical/thermal land surface parameters (MODIS) and meteorological forcing (ERA5-Land), using a random forest algorithm trained on extensive ground observations. ~~Specifically, it downscales and fuses coarse-resolution passive microwave observations (AMSR-E/2) with high-resolution optical/thermal land surface parameters (MODIS) and meteorological forcing (ERA5-Land), using a random forest algorithm trained on extensive ground observations.~~

Validation and Uncertainty: This product was selected for its capacity to resolve hillslope-scale heterogeneity in complex terrain, a critical requirement for our hazard-focused analysis. Comprehensive validation against approximately 2,400 in-situ stations across China demonstrates robust accuracy, with an average correlation coefficient (R) of 0.89 and an unbiased Root Mean Square Error (ubRMSE) of 0.053 m^3/m^3 (Song et al., 2022). While inherent uncertainties exist in~~we acknowledge the inherent uncertainties associated with~~ microwave retrieval in mountainous regions

(e.g., geometric distortion and shadowing effects), this dataset represents the biases~~state-of-the-art~~ balance between spatial resolution and temporal continuity. Furthermore, since our study focuses on the temporal persistence features (spectral exponents) rather than absolute magnitudes, the potential systematic bias in complex terrain has minimal impact on the derived memory metrics (see Appendix C for further discussion on data reliability and preprocessing).

Table 1. Static and dynamic covariates used in the final modeling framework and the target variable (soil moisture, SM).

Types	Variable (abbreviation)	Description	Units	Source
Static	Slope (~~$\theta\beta$~~)	Rate of change of elevation at each pixel (DEM-derived)	°	Geospatial Data Cloud (DEM)
	Aspect (Asp)	Orientation of the steepest downslope (DEM-derived)	°	
	Topographic Wetness Index (TWI)	Potential wetness index based on slope and upslope contributing area (DEM-derived)	-	
	Soil texture (Sand, Silt, Clay)	Mass fractions of soil particle-size classes	g/kg	Soil Grids
	Normalized Difference Vegetation Index (NDVI)	Vegetation greenness from red and NIR reflectance	-	Gao et al., 2022
Dynamic	Precipitation (Prec.)	Daily total precipitation	mm	Xie et al., 2019
	Surface wind speed (WS)	Mean daily wind speed at 10 m height	m/s	ERA5 (Hersbach et al., 2023)
	Relative humidity (rhu)	Ratio of actual to saturated vapor pressure	%	
	2m air temperature (T_{2m})	Daily mean air temperature at 2 m height	℃	
	Actual evaporation (AE)	Daily actual evapotranspiration	mm/day	
Target	Soil moisture (SM)	Volumetric soil water content	cm^3/cm^3	Song et al., 2022

~~Auxiliary s~~Static variables (e.g., soil texture, TWI) represent basin physiography, while

dynamic variables (e.g., precipitation, NDVI) capture climate-vegetation interactions. All data were resampled to a uniform 1-km grid. Preprocessing included linear interpolation for short gaps (≤ 3 days), outlier removal, and stationarity checks using the Augmented Dickey-Fuller test (details in Appendix C).

2.3 Quantifying Soil Moisture Memory (PSA and DFA-2)

To characterize the multi-scale persistence of soil moisture, we employed two complementary spectral techniques that quantify long-range temporal correlations. ~~-~~ Power Spectrum Analysis (PSA) identifies memory strength across frequency domains, while Detrended Fluctuation Analysis (DFA-2) detects the timescales over which memory persists. Both methods are robust to non-stationarity and can distinguish genuine long-term correlations from short-term noise or trends (Kantelhardt et al., 2006; Zhu et al., 2010). ~~Crucially, g~~

Given the 20-year record length~~length of our dataset~~ (2003 – 2022), ~~distinct~~ statistical limitations exist for resolving low-frequency dynamics. Following established guidelines in spectral requiring ~~the standard signal processing constraint which requires the time series length (N) to be significantly longer than the timescale of interest (T) for robust estimation (typically~~ $N \geq 3T$ for robust spectral estimation (Ghannam et al., 2016; Percival & Walden, 1993), we ~~explicitly~~ distinguish between two regimes:

1. **Reliable Spectral ~~Memory~~ Window ($T \leq 7$ years):** Timescales up to $T = N/3 \approx 6.7$ years (rounded to 7 years) can be reliably estimated, as our record contains at least three complete cycles. ~~Timescales where sufficient realizations (approx. N/3) exist to statistically verify dynamic persistence and oscillatory behavior.~~
2. **Low-Frequency Background State ($T > 7$ years):** Signals at these timescales reflect

slow-varying boundary conditions (e.g., multi-year drought periods) rather than event-scale memory. These estimates have lower statistical confidence and are interpreted as qualitative indicators of long-term storage trends.~~The lowest frequency components, which are interpreted as basin storage trends or decadal climatic regime shifts, rather than verifiable memory cycles.~~

Power Spectral Analysis (PSA). PSA decomposes a time series into its constituent frequencies, estimating how variance (power) is distributed across them. The relationship follows a power law: $S(f) \sim f^{-\beta}$, where $S(f)$ is the spectral power at frequency f, and β is the spectral exponent. A higher β indicates that low-frequency (long-term) variations dominate the signal, implying stronger soil moisture memory. In this study, β values within the Reliable Spectral Window (seasonal to ~7 years) quantify interannual persistence, while those in the Low-Frequency Background (>7 years) indicate quasi-static mean-state stability.

~~First, Power Spectrum Analysis (PSA) was utilized to diagnose the strength of temporal memory in the frequency domain. By estimating the spectral exponent (β), PSA effectively distinguishes memory-driven processes (red noise, $\beta > 0$) from random meteorological inputs (white noise, $\beta \approx 0$). In this study, β values derived within the Reliable Memory Window (seasonal to ~7 years) are used to quantify interannual persistence, whereas values in the Low-Frequency Background (> 7 years) serve only as indicators of the quasi-static mean-state stability.~~

Detrended Fluctuation Analysis (DFA-2). To account for non-stationarity, we applied second-order DFA-2. It quantifies long-range correlations by analyzing how the root-mean-square fluctuation $F(s)$ of the integrated series scales with window size s: $F(s) \sim s^{\alpha}$. The fluctuation exponent α indicates the correlation structure: $\alpha = 0.5$ corresponds to uncorrelated white noise; $\alpha >$

0.5 indicates persistent long-range correlations; and α = 1.0 represents scale-invariant 1/*f* noise (Kantelhardt et al., 2001). DFA-2 filters out polynomial trends to reveal intrinsic correlations, making it suitable for non-stationary hydrological records. Cross-validation with the standard Autocorrelation Function confirms the robustness of these metrics (Appendix E, Fig. E1). ~~Second, to account for the non-stationarity inherent in long-term hydrological records, we applied the second-order Detrended Fluctuation Analysis (DFA-2). Unlike standard autocorrelation, DFA-2 filters out polynomial trends to reveal intrinsic correlation structures. Cross-validation with the standard Autocorrelation Function (ACF) further confirms the robustness of these DFA-2 metrics (see Fig. E1 in Appendix).~~

We defined the "persistence horizon" as the range of timescales over which $\alpha \geq 0.9$, indicating strong long-range memory approaching scale-invariant behavior. In this study, persistence horizon is used as the operational measure of memory length, specifically denoting the temporal range where significant long-range memory ($\alpha \geq 0.9$) is maintained. This threshold follows established criteria in hydroclimatic memory studies (Zhang et al., 2025; Zhu et al., 2010). Physically, it represents the temporal window over which antecedent moisture conditions influence the current state—a critical parameter for hazard preconditioning. Persistence horizons extending beyond 7 years reflect slow-changing baseline conditions rather than event-scale memory. Detailed formulations and significance testing are provided in Appendix A.~~We specifically identified "persistence horizons" — time windows where the fluctuation exponent (α) exceeds 0.9. Consistent with the PSA framework defined above, persistence horizons extending beyond the 7-year threshold are classified as "Background Preconditioning" baselines, distinct from the active dynamic memory observed at shorter scales. Detailed mathematical formulations, including the phase-randomization significance~~

~~testing, are provided in Appendix A.~~

For clarity, key terms are defined as follows:

- **Soil Moisture Memory (SMM):** The tendency of soil moisture anomalies to persist over time following wetting or drying events. SMM is quantified by the spectral exponent β (memory strength) and fluctuation exponent α (memory timescale).
- **Significant Memory:** A state where $\alpha \geq 0.9$, indicating strong long-range correlations.

Persistence Horizon: The timescale range (in days) over which significant memory is observed.

2.4 Identifying Predictors via a Spatial Attribution Modeling Framework

To determine the hierarchical importance of environmental predictors, we utilized the Boruta feature selection algorithm wrapped around a Random Forest regressor. Boruta is an all-relevant feature selection method that creates randomized "shadow" copies of original predictors (permuted versions with no real relationship to the target) and iteratively compares the importance of each real predictor against the best-performing shadow variable. Predictors that consistently outperform shadow variables are retained as relevant, while others are rejected (Kursa & Rudnicki, 2010). Boruta was selected because it (1) captures non-linear relationships inherent in soil-vegetation-atmosphere systems, (2) handles collinearity among predictors without requiring prior variable removal, and (3) provides statistically validated importance rankings by comparing against a null model.

Given that SMM is a temporal statistic derived from time series, while landscape attributes are spatially heterogeneous, we constructed a spatial attribution framework to link these dimensions, quantifying how driver importance shifts across different temporal aggregation windows (monthly

to decadal). Specifically, the temporal memory metric for each pixel (e.g., spectral exponent β) serves as the spatial response variable, regressed against spatially distributed predictors: ~~Given that SMM is a temporal statistic derived from time series, while landscape attributes are spatially heterogeneous, we constructed a spatial attribution framework to link these dimensions.~~

~~In this approach, the temporal memory metric calculated for each pixel (e.g., the spectral exponent β) serves as the spatial response variable. This target was regressed against a suite of spatially distributed predictors, which were categorized into two groups:~~

1. **Static variables:** Landscape properties that remain constant over the study period (e.g., soil texture, slope, TWI).
2. **Aggregated dynamic variables:** Time-varying meteorological and vegetation data aggregated to match the temporal scale of the memory metric (e.g., mean decadal NDVI or total precipitation).

This construction allows us to quantify how spatial heterogeneity in static and dynamic boundary conditions correlates with the temporal persistence of soil moisture. Feature importance was validated using spatial block cross-validation to account for spatial autocorrelation (details in Appendix D).

2.5 Methodological Considerations and Limitations

The "Space-for-Time" framework leverages spatial heterogeneity across the three watersheds as a substitute for long-term temporal observations at a single site, an approach widely adopted in ecological and hydrological studies (Pickett, 1989). However, this approach identifies statistical associations rather than causal relationships. The Boruta-RF algorithm ranks predictors by their capacity to explain spatial variance in temporal memory metrics, but cannot distinguish between

direct causal drivers, proxy variables, or feedback responses. Therefore, associations should be interpreted as indicative of likely controls rather than confirmed causal mechanisms (McColl et al., 2017; Seneviratne et al., 2010).

Additionally, physical collinearity inherent in mountain landscapes—often described by the catena concept of co-evolved soil-topography relationships (i.e., steep upper slopes have thin, sandy, fast-draining soils while gentle lower slopes accumulate thick, clay-rich, water-retaining soils; Anderson, 2005)—means that high importance scores for both Slope and Clay content (Section 3.3) likely reflect coupled landscape structure rather than independent effects.

~~It is essential to emphasize that the "Space-for-Time" framework employed here identifies statistical associations rather than establishing causal relationships. The Boruta-RF algorithm ranks predictors by their capacity to explain spatial variance in temporal memory metrics, but fundamentally cannot distinguish between: (i) direct causal drivers, (ii) proxy variables correlated with unmeasured causal factors, or (iii) response variables involved in bidirectional feedback loops.~~

To address these limitations, we (1) interpret associations through established hydrological theory (e.g., linear reservoir models; Section 4.1) to provide mechanistic plausibility, and (2) conduct partial correlation analysis controlling for topographic variables (Appendix G) to assess robustness against landscape confounding. This framework generates testable hypotheses about SMM predictors rather than confirming causal mechanisms, which would require controlled experiments beyond the scope of this study.

~~Furthermore, the physical collinearity inherent in mountain landscapes—often termed the "catena concept"—means that soil texture and topography co-evolve along hillslopes: steep upper slopes typically develop shallow, coarse-textured soils with rapid drainage, whereas convergent~~

~~lower slopes accumulate deep, clay-rich deposits with enhanced water retention. Consequently, high importance scores for both Slope and Clay content (Section 3.3) likely reflect this coupled landscape structure rather than fully independent effects.~~

~~To partially address these limitations, we: (1) interpret the identified associations through the lens of established hydrological theory (e.g., linear reservoir models; Section 4.1), providing mechanistic plausibility for the observed statistical patterns; and (2) conduct partial correlation analysis controlling for topographic variables (Appendix G) to assess the robustness of soil-SMM associations against landscape confounding. However, readers should note that our framework is designed to generate testable hypotheses about SMM predictors rather than to confirm causal mechanisms, which would require controlled experiments or instrumental variable approaches beyond the scope of remote sensing analysis.~~

3. Results

3.1 Power Spectrum Analysis of SM Memory

Power spectrum analysis revealed scale-dependent characteristics of soil moisture memory (SMM) across the three basins (Fig. 3). Quantitative interpretations focus on the Reliable Spectral Window (≤ 7 years), while longer timescales reflect quasi-stationary moisture regimes.~~It is important to note that while spectral analyses are presented up to the 20-year scale to illustrate trends, quantitative interpretations are explicitly distinguished based on the record length constraint. We define the 1–7 year range as the "Reliable Spectral Window" for dynamic memory estimation ($N \geq 3T$). Results beyond this threshold (> 7 years) are interpreted as the "Low-Frequency Background State," reflecting the system's convergence to equilibrium rather than oscillatory persistence.~~

In Figure 3, the x-axis represents frequency (cycles per year, logarithmic scale) and the y-axis

represents spectral power $S(f)$ (log-transformed). The spectral exponent β corresponds to the negative slope of the fitted line: higher β indicates variance concentrated at low frequencies, implying strong memory, while lower β indicates high-frequency dominance characteristic of weak memory. Shaded bands represent 95 % confidence intervals. Three key patterns emerge: (1) intra-annual contrasts between wet and dry seasons, (2) systematic decline in memory strength with increasing timescale, and (3) inter-basin differences reflecting contrasting hydro-climatic regimes. For seasonal classification, the rainy and dry seasons are defined based on local precipitation regimes: the Dali River Basin (DRB) rainy season spans July to September (dry season: October–June), while both the Anning River Basin (ARB) and Jiangjia Ravine (JJR) share a rainy season from May to October (dry season: November–April).

Intra-annual patterns: Analysis compared individual months with integrated seasonal periods (Fig. 3a–1, b–1, c–1). This revealed asymmetric patterns: memory during individual rainy season months was consistently weaker than the integrated rainy season, whereas individual dry season months showed stronger memory than the dry season aggregate. For example, in the ARB, the integrated rainy season yielded $\beta = 2.190 \pm 0.101$, while individual rainy months averaged $\beta = 2.179 \pm 0.095$; conversely, individual dry season months ($\beta = 2.698 \pm 0.121$) exceeded the integrated dry season ($\beta = 1.643 \pm 0.051$).

Interannual patterns: SMM declined progressively at longer timescales. Within the reliable window, the hierarchical trend follows β(1-yr) > β(5-yr). Beyond 7 years, metrics stabilized, capturing the basin's static storage baseline (Fig. 3a–2, b–2, c–2). ~~Power spectrum analysis revealed the scale-dependent characteristics of soil moisture memory (SMM) across the three basins (Fig. 3). All reported spectral exponents (β) are presented as the mean estimate ± the 95 % confidence~~

~~interval derived from the log-log regression. Extensive sensitivity tests (detailed in Appendix E, Table E4 and Fig. E2) further confirm that these spectral patterns are robust to variations in detrending orders and frequency cutoffs, with the spatial ranking of memory strength remaining highly consistent (Spearman's $\rho > 0.92$) across parameter sets.~~

~~At short timescales (within one year), memory during individual rainy season months was consistently weaker than that of the integrated rainy season period, whereas dry season months showed stronger memory than the overall dry season aggregate (Fig. 3a–1, b–1, c–1).~~

~~Over longer intervals (1–20 years), SMM declined progressively. Within the reliable window, the hierarchical trend generally follows $\beta_{1\text{-yr}} > \beta_{5\text{-yr}}$. Beyond this point, in the low-frequency background zone (> 7 years), the metrics stabilized, capturing the basin's static storage baseline (Fig. 3a–2, b–2, c–2).~~

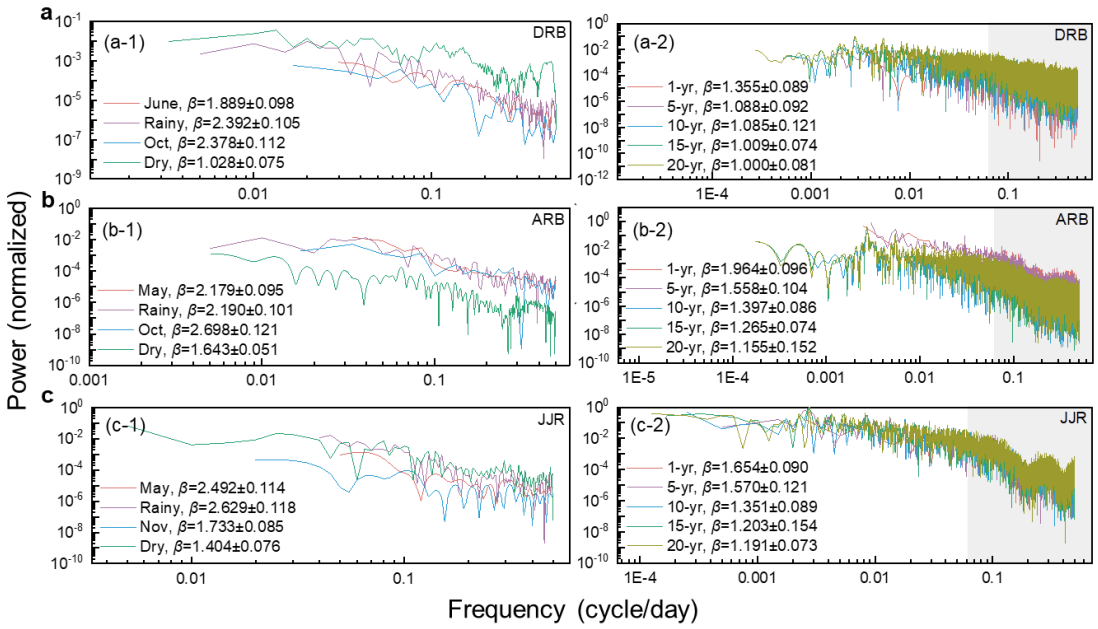

Fig. 3 Power spectrum analysis of soil moisture memory in the (a) Dali River Basin (DRB), (b) Anning River Basin (ARB), and (c) Jiangjia Ravine (JJR). Left panels show intra-annual ~~normalized power~~ spectra ~~at intra-annual scales~~ (months and aggregated seasons~~). ~~); ~~Right~~ right panels show

inter-annual spectra (1 ~ 20 years). The spectral exponent β(~~β,~~ mean ± 95% CI) is derived from linear regression in log-log space, where steeper slopes indicate stronger memory. Gray shading denotes timescales >1825 days, where spectral estimation is limited by record length; estimates beyond the ~7-year scale should be interpreted as low-frequency background trends rather than statistically robust memory features. Key findings: rainy season memory exceeds dry season memory; β decreases with increasing timescale; ARB shows the strongest memory, followed by JJR and DRB.~~quantifies memory strength, with higher values indicating stronger long-term persistence. The gray-shaded region (Time Scale > 1825 days) denotes where spectral estimation is limited by the 20-year data record; results here should be interpreted as low-frequency trends rather than robust spectral features. CI, confidence interval.~~

In the Dali River Basin (DRB), ~~the~~ full rainy season memory (β = 2.392 ± 0.105)~~, calculated over the continuous period from June to September,~~ was significantly stronger than ~~that of~~ the initial month (June, β = 1.889 ± 0.098), indicating pronounced long-range persistence where cumulative monsoon rainfall progressively builds hydrological inertia (Rahmati et al., 2024). Conversely, integrated dry season memory (β = 1.028 ± 0.075) was weaker than October (β = 2.378 ± 0.112) (Fig. 3a-1), reflecting residual moisture persisting into early autumn before rapid depletion. At interannual scales, SMM declined from β = 1.355 ± 0.089 (1-year) to β = 1.000 ± 0.081 (20-year)~~In contrast, the integrated dry season memory (β = 1.028 ± 0.075) was considerably weaker than that of October (β = 2.378 ± 0.112) (Fig. 3a-1). At interannual scales, SMM systematically declines from β = 1.355 ± 0.089 (1-year) to β = 1.000 ± 0.081 (20-year) (background state)~~ (Fig. 3a-2~~).~~), indicating limited carryover beyond a few years. For erosion hazards, antecedent moisture from preceding weeks to months—rather than years—is most relevant for modulating soil erodibility (Ran et al., 2012).

In the Anning River Basin (ARB), ~~the~~ integrated rainy season memory (β = 2.190 ± 0.101) ~~is~~

was slightly stronger than that of May (β = 2.179 ± 0.095), peaking in October (β = 2.698 ± 0.121) (Fig. 3b-1). High β values reflect strong persistence driven by accumulated monsoon precipitation and the buffering capacity of deep forest soils (Bogaard & Greco, 2018). At interannual scales, the ARB exhibitedhad the highest SMM among the basins, with a (mean β of 1.468 ± 0.084), exceeding the DRB (1.107 ± 0.072) and JJR (1.394 ± 0.079) and decreased decreasing gradually from 1.964 ± 0.096 (1-year) to 1.265 ± 0.074 (20-year) (background state) (Fig. 3b-2). This sustained multi-year memory suggests wet years can progressively elevate baseline pore pressures, potentially lowering landslide triggering thresholds (Cui et al., 2025).

In the Jiangjia Ravine (JJR), SMM peakeds during the rainy season (May: β = 2.492 ± 0.114; full rainy season: β = 2.629 ± 0.118), whereas it and weakened during the dry season (Nov: β = 1.733 ± 0.085; full dry season: β = 1.404 ± 0.076) (Fig. 3c-1). This strong seasonal contrast reflects rapid hydrological response: frequent monsoon rainfall maintains elevated moisture and strong autocorrelation, while steep terrain promotes quick drainage during dry periods. At interannual scales, the JJR exhibited an intermediate level of SMM — stronger than that of the DRB but weaker than the ARB — with β values decreasing from 1.654 ± 0.090 (1-year) to 1.191 ± 0.073 (20-year) (background state) (Fig. 3c-2). For debris flow hazards, antecedent wetness from preceding days to weeks within the rainy season is critical (Wei et al., 2025), whereas inter-annual carryover is less pronounced than in the forest-buffered ARB.

In summary, SMM is consistently stronger in rainy seasons than in individual months and weakens progressively toward a climate-driven baseline. The ARB shows the strongest overall memory, highlighting how basin characteristics shape persistence beyond short-term weather effects—with clear relevance for multi-scale hazard prediction.

3.2 DFA-2 Analysis of SM Persistence Horizons

Building on the~~Based on the memory characteristics identified by~~ PSA results, we ~~next~~ quantified ~~the associated~~ persistence horizons using DFA-2. While β characterizes overall memory strength, the fluctuation exponent α identifies specific timescales where memory is strongest ($\alpha \geq 0.9$). All reported α values in this range were statistically significant ($p < 0.01$) based on phase-randomization surrogate testing (see Appendix A). ~~All reported α values in the high-memory range ($\alpha \geq 0.9$) were statistically significant ($p < 0.01$) based on phase-randomization surrogate testing (see Appendix A).~~

Figure 4 presents DFA-2 results organized by basin (rows: a = DRB, b = ARB, c = JJR) and timescale (columns: left = seasonal, right = inter-annual). Solid lines show how α varies with window size s; labeled time windows (e.g., "236–728 d") indicate persistence horizons where $\alpha \geqslant 0.9$.

~~Soil moisture persistence exhibited distinct spatiotemporal patterns across the three basins (Fig. 4).~~ In the Dali River Basin (DRB), persistence was short during the early rainy season (24-30 days in June) but extends substantially through the full rainy season (41-122 days); ~~in contrast,~~ October exhibited negligible persistence, with α falling below the 0.9 threshold (Fig. 4a-1). This indicates rapid decay of moisture anomalies due to intense evaporative drying following monsoon withdrawal. During the dry season, persistence increased to 61–95 days, reflecting conditions where moisture decay is governed primarily by intrinsic drainage properties rather than evaporative demand (Seneviratne et al., 2010). At interannual scales, persistence horizons increased from 31–73 days (1-year) to 174–429 days (20-year), peaking between 10 and 15 years (Fig. 4a-2). This pattern is

consistent with deeper-layer memory and reduced influence of high-frequency atmospheric forcing at longer timescales (Rahmati et al., 2024).~~October showed almost no persistence (Fig. 4a-1). During the dry season, persistence increased to 61-95 days, indicating a stronger influence of soil properties under limited rainfall. Beyond the seasonal scale, the characteristic persistence horizon increased moderately from 31-73 days (1-year) to 174-429 days (20-year), peaking between 10 and 15 years (Fig. 4a-2).~~

The Anning River Basin (ARB) exhibited the longest persistence horizons across all temporal scales~~, with all reported ranges being statistically significant~~ ($p < 0.05$)~~ based on the DFA-2 significance testing procedure described in Section 2.4 (2)~~. At the monthly scale, persistence ranged from 17-31 days in May to 25–31 days in October, increasing~~and these durations increased~~ markedly at the seasonal scale—reaching 37-184 days during the rainy season and 47-76 days during the dry season (Fig. 4b-1). At interannual scales~~Beyond the seasonal scale~~, ~~the~~ persistence horizons rose sharply from 40-71 days (1-year) to 236-728 days (20-year) (Fig. 4b-2). This extended memory implies that the basin's soil moisture state integrates cumulative effects of multi-year climate variability rather than responding solely to individual storm events. Consequently, a sequence of wet years progressively saturates deep soil layers, elevating background pore pressures—a critical factor for landslide susceptibility assessment.~~window, particularly at the multi-year scale, implies that the basin's soil moisture state tracks the low-frequency signals of inter-annual climate oscillations and vegetation dynamics (i.e., red noise spectra of forcing). This persistence indicates a shift in the hydrological equilibrium rather than physical water retention, thereby conditioning the baseline hydrological state for hazard susceptibility over multiple years.~~

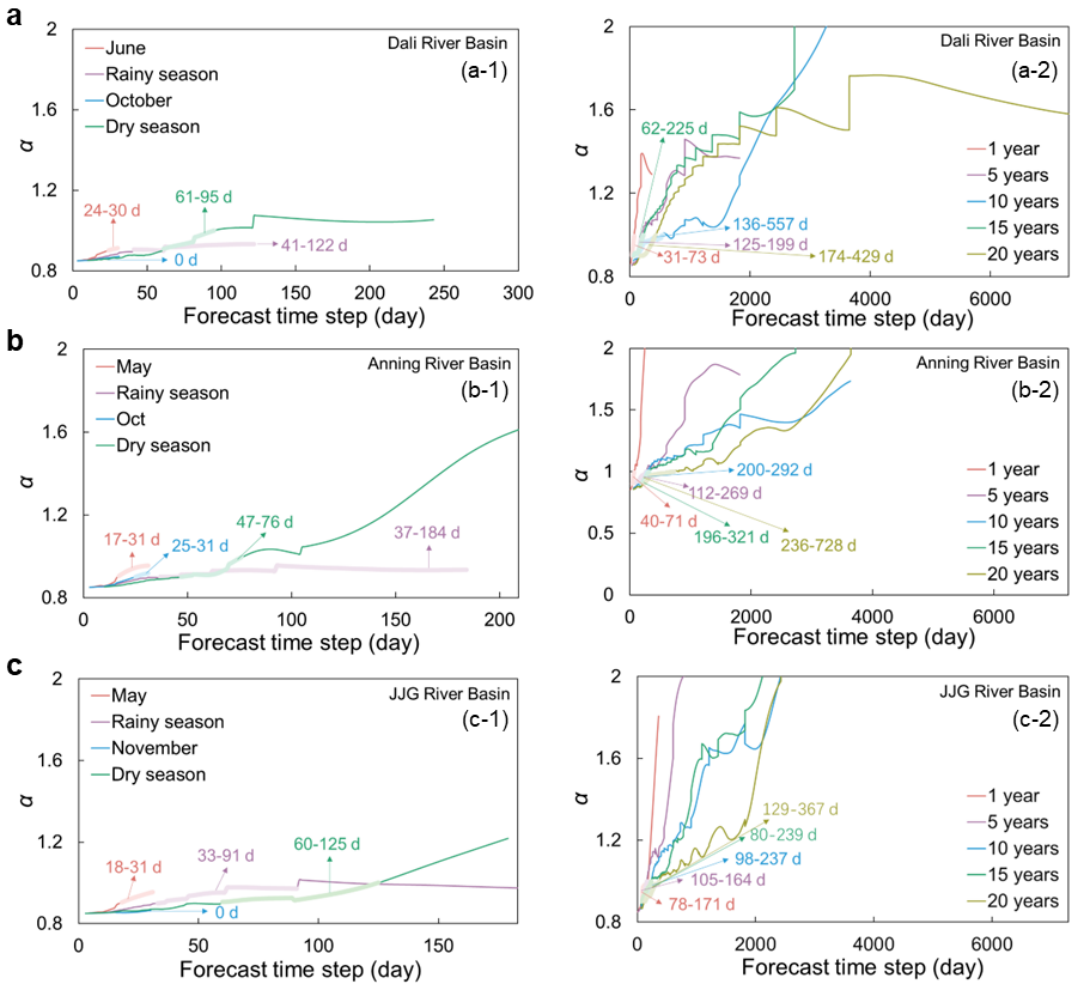

Fig. 4 DFA-2 analysis of soil moisture persistence across ~~the three basins.~~ : (a) Dali River Basin (DRB), (b) Anning River Basin (ARB), and (c) Jiangjia Ravine (JJR). Left panels ~~show~~: seasonal scales; ~~Right~~ right panels: ~~show~~ inter-annual scales (1~~, 5, 10, 15, and~~ -20 years). Solid lines represent the ~~DFA-2~~ fluctuation exponent (α), ~~calculated using a window size range of $s \in [10, N/4]$ days (where N is the series length). The~~ labeled time windows indicate persistence horizons where $\alpha \geq 0.9$. ARB shows the longest persistence (up to 728 days), JJR the shortest rainy-season persistence (18–31 days), and DRB intermediate values. Sensitivity tests are detailed in Appendix E. ~~(e.g., "236-728 d") define the characteristic persistence horizons—the range of timescales over which significant memory ($\alpha \geq 0.9$) is observed. Sensitivity tests confirming the robustness of these horizons against window size variations (e.g., $N/8$) are detailed in Appendix E. d: days.~~

In the Jiangjia Ravine (JJR), rainy season persistence was the shortest among the three basins (18-31 days in May; 33-91 days when aggregated), indicating ~~a~~ rapid response to precipitation

inputs (Fig. 4c-1). This 2–4 week persistence horizon defines the critical "look-back window" for debris flow early warning (Pan et al., 2018; Wicki et al., 2020). In contrast, dry season persistence (60 – 125 days) was longer, reflecting reduced evaporative demand when rainfall ceases. At interannual scales, persistence horizons remained stable, ranging from 78–171 days (1-year) to 129–367 days (20-year) (Fig. 4c-2), suggesting that intrinsic drainage characteristics impose a consistent upper bound on moisture retention regardless of climatic variability. ~~In contrast, dry season persistence (60–125 days) is longer than that in the ARB but remains shorter than in the DRB. At interannual scales, persistence horizons exhibit remarkable stability, ranging from 78–171 days (1-year) to 129–367 days (20-year) (Fig. 4c-2), suggesting a consistent memory effect across long-term timescales.~~

Persistence horizons vary markedly across basins: longest in ARB (months to years), shortest in JJR during the rainy season (2–4 weeks), and intermediate in DRB. These time windows define practical "look-back" periods for anticipating different mountain hazards, from short-term debris flows to longer-term landslide preconditioning.

3.3 Driving Factor Selection

The Boruta Random Forest Algorithm identified statistical associations between environmental variables and SMM across multiple timescales~~(BRFA) was employed to evaluate the statistical associations between dynamic variables and SMM across multiple timescales, providing quantitative insights into the factors most strongly correlated with SM variability at different temporal resolutions~~ (Fig. 5). Variables were classified as "confirmed" (*Z*-score significantly exceeds shadow maximum, $p < 0.01$), "tentative" (borderline significance), or "rejected." Bootstrap resampling ($n = 1000$) confirmed that top predictors at each scale maintained significance across >

95% of iterations. ~~Bootstrap resampling (n = 1000) confirmed that the top 3 predictors at each scale maintained significance across > 95 % of iterations, whereas tentative variables showed high variability (CV > 40 %), validating our interpretation focus on confirmed factors.~~

M~~At the m~~onthly to seasonal scale~~,~~: June—the onset of the rainy season—showed no distinct dominant predictor~~;~~. ~~h~~However, when the entire rainy season (Jun-Sep) ~~is~~ was considered, relative humidity (rhu), NDVI, actual evaporation (AE), and 2-m air temperature (T_{2m}) emerged as the strongest statistical predictors of SMM spatial patterns. During the dry season (Oct-May), ~~the hierarchy of predictive associations shifted notably. In October,~~ NDVI, AE, rhu, and T_{2m} maintained strong correlations with SMM, whereas precipitation and wind speed exhibited limited predictive power~~.~~, ~~This shift likely reflects~~ reflecting the transition from moisture-limited to energy-limited evapotranspiration regimes.

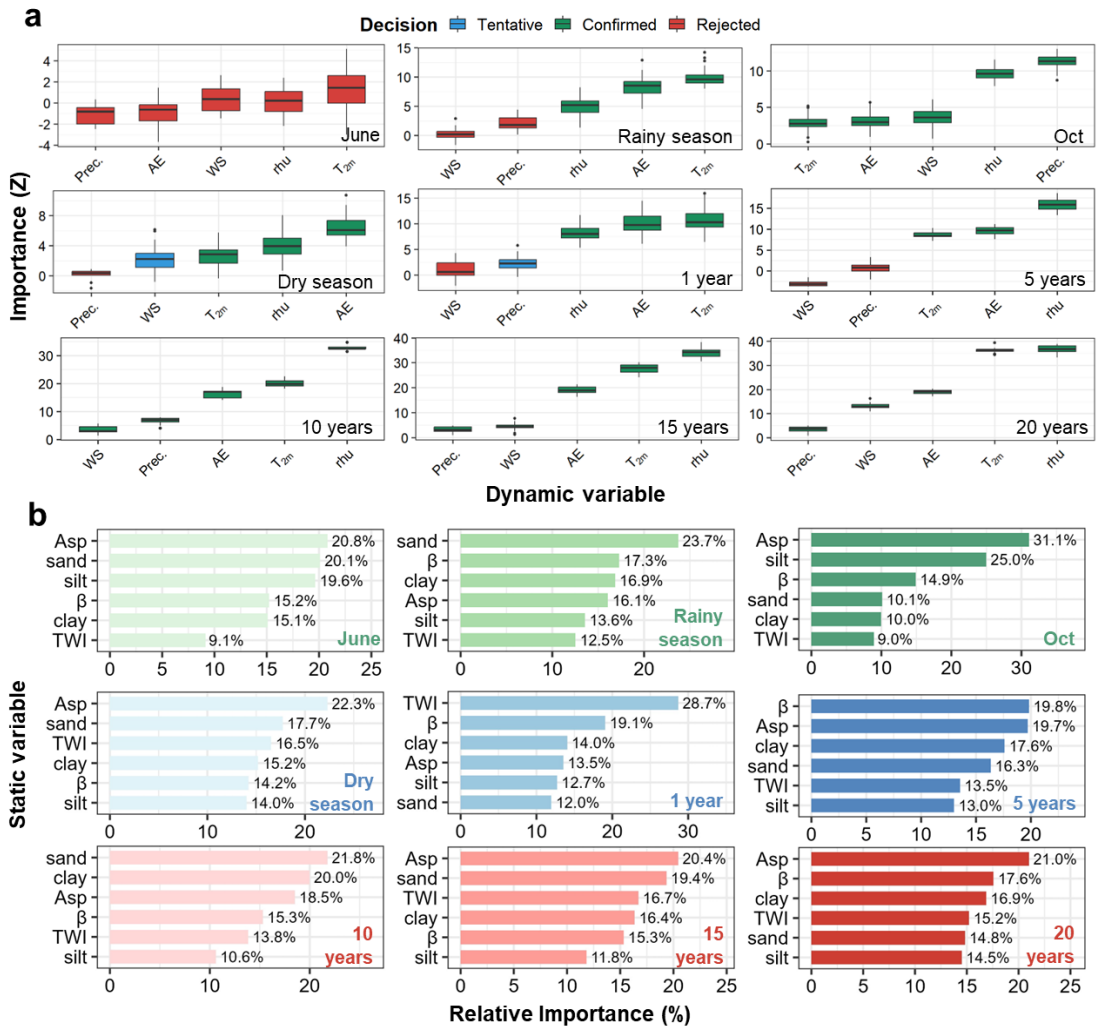

Fig. 5 Scale-dependent predictive importance of environmental drivers for soil moisture memory from monthly to decadal timescales. (a) Dynamic drivers evaluated by Boruta algorithm (*Z*-scores; green: confirmed, yellow: tentative, red: rejected; $p < 0.01$). (b) Static drivers assessed by Random Forest (relative importance, %). Note: Panels (a) and (b) use different metrics and are not directly comparable. Abbreviations: Prec., precipitation; WS, wind speed; rhu, relative humidity; T_{2m}, 2-m air temperature; AE, actual evapotranspiration; NDVI, normalized difference vegetation index; TWI, topographic wetness index; Asp., aspect; ρ_b, bulk density.

~~. (a) Dynamic drivers (Boruta Z-scores), where green boxes denote confirmed variables ($p < 0.01$). (b) Static drivers (Random Forest Relative Importance, %). ***Note***: Panels (a) and (b) use different metrics (unbounded Z-scores vs. normalized percentages); thus, absolute magnitudes are not directly comparable.~~

Annual to decadal scales: T~~At longer timescales, t~~he pattern of statistical associations

underwent ~~a~~ progressive transition.~~:~~ The cumulative importance of atmospheric variables (Precipitation, Wind Speed, T_{2m}, rhu) declined from 62 % at the monthly scale to 34 % at the 10-year scale, while soil texture variables (Sand, Silt, Clay) increased from 12 % to 38 % (Fig. 5).~~–~~ ~~On an~~At annual scale, precipitation and wind speed~~—whose association with SMM stems from event-scale forcing—~~ declined in importance as temporal averaging smooth~~s out~~ed their high-frequency variability. By the 5-year scale, these climatic variables were ~~fully~~ excluded from ~~the set of~~ significant predictors, leaving NDVI, rhu, AE, and T_{2m} as dominant~~the~~ variables~~ most strongly associated with SMM variability~~. Over decadal timescales (10–20 years), ~~the~~ associations of NDVI, rhu, and T_{2m} with SMM further intensified~~, highlighting their persistent correlation with long-term SM dynamics~~.

Static factors: The relative importance of static factors also varied with timescale~~The relative importance of static factors also exhibited distinct temporal patterns~~ (Fig. 5b). During June and the rainy season, bulk density (ρ_b~~ρb~~) and aspect (Asp) showed the strongest associations~~ with SM~~. At the annual scale, ~~the pattern shifted slightly toward stronger~~ topographic associations (TWI) strengthened. However, over longer timescales, pedological factors became increasingly prominent ~~in the predictor hierarchy~~.

Scale-transition threshold: Quantitative analysis~~Quantitative analysis of the feature importance~~ revealed a distinct structural break at the 5-year scale (Table 2~~ and Fig. 5~~). At the 1-year scale, ~~the system showed the strongest association with~~ TWI showed the strongest association (28.7 %), consistent with topography-driven lateral redistribution~~lateral redistribution processes~~. ~~However,~~ ~~a~~At the 5-year scale, TWI importance declined~~collapsed~~ (to 13.5 %), ~~and~~ with the hierarchy ~~shifted~~ shifting to ~~a stable group of~~ Soil Texture and Slope (~ 19 %). This~~We therefore operationally define~~

~~the 5-year scale as the critical transition~~ threshold~~,~~ reflects a fundamental shift from event-scale hydraulic connectivity ("Fast-Response Regime") to long-term pedological storage control ("Background-Storage Regime") (Blöschl & Sivapalan, 1995; Western et al., 2004). ~~as it marks the precise timescale where the association pattern transitions from TWI-dominated ('Fast-Response Regime') to Soil-dominated ('Background-Storage Regime').~~

~~It is important to note that these associations do not establish causal relationships. The Boruta-RF algorithm identifies variables with strong predictive power for SMM spatial patterns, but cannot distinguish between direct causal drivers, proxy variables, or variables involved in bidirectional feedbacks. For instance, the strong association between NDVI and SMM at decadal scales may reflect vegetation's influence on soil hydraulic properties, soil moisture's constraint on vegetation growth, or both operating within a coupled ecohydrological system. The mechanistic interpretation of these statistical patterns is discussed in Section 4.1.~~

Table 2. The structural shift in dominant statistical associations~~dominant environmental associations~~ across timescales.

Time Scale	Top Static Predictor (Importance %)	Top Dynamic Predictor (Importance *Z*)	Association Pattern
1-Year	TWI (28.7%)	T_{2m} (11.2)	Topography-Associated (Water redistribution)
5-Year	*β*/Asp (~19.8%)	rhu (16.1)	Transition Point (TWI collapses; Structure stabilizes)
10-Year	Sand (21.8%)	rhu (32.5)	Soil-Texture Associated (Storage capacity)
20-Year	Asp (21.0%)	rhu (36.2)	Soil-Texture Associated

***Note*:** Seasonal scales (e.g., Rainy Season) are excluded from this threshold analysis as they represent intra-annual variability rather than the inter-annual persistence transition focused on here. "Predictor" and "Associated" terminology is used to reflect statistical relationships; causal interpretations require additional mechanistic validation (see Section 2.4 and Section 4.1).

Methodological considerations: These associations do not establish causal relationships. The

Boruta-RF algorithm identifies variables with strong predictive power but cannot distinguish between direct causal drivers, proxy variables, or bidirectional feedbacks. For instance, the strong NDVI–SMM association at decadal scales may reflect vegetation's influence on soil hydraulic properties, soil moisture's constraint on vegetation growth, or both. Mechanistic interpretation is discussed in Section 4.1.~~To assess the robustness of these associations against potential confounding by landscape collinearity (the "catena effect," whereby soil properties and topography co-evolve), we conducted p~~ Partial correlation analysis controlling for topographic variables (Appendix G)~~. Results~~ indicated that soil texture maintained significant partial correlations with decadal-scale SMM (partial $r = 0.43$, $p < 0.01$) ~~even~~ after accounting for slope and TWI, though ~~the~~ effect size was reduced compared to the raw correlation ($r = 0.61$~~). ~~)~~, This suggests~~ suggesting ~~that~~ approximately 30 % of the apparent ~~soil texture~~ association may be attributable to topographic confounding~~, while the remaining signal likely reflects genuine pedological influences on moisture retention~~.

~~We therefore define the 5-year scale as the critical threshold where the predictive importance of static landscape variables supersedes that of high-frequency dynamic forcing. These findings underscore the statistical interplay between static and dynamic predictors and emphasize the need to incorporate multiscale factors into early-warning systems.~~

Short-term memory is driven primarily by weather and vegetation factors, whereas beyond ~5 years, soil texture and topography become dominant. This scale-dependent shift from dynamic to static control marks a fundamental transition in SMM mechanisms—essential for developing timescale-appropriate hazard models.

3.4 Cross-Basin Comparison of Memory and Drivers

To ~~directly~~ address ~~the~~ basin-specific memory characteristics relevant to~~of~~ mountain hazards, we synthesized ~~and compared the~~ SMM characteristics properties and dominant controls across the three watersheds ~~at representative temporal scales (monthly, annual, and decadal)~~. The key metrics—spectral exponent (β), DFA-2 predictive period, and the top three driving factors—at ~~representative temporal scales (~~monthly, annual, and decadal scales~~)~~ are summarized in Table 3. Complete~~This synthesis highlights the basin-specific hierarchies, while the complete, scale-explicit results of the~~ Boruta and Random Forest results~~analyses~~ for the ARB and JJR provided~~are available~~ in Appendix F (Figs. F1-F4)~~, respectively~~.

Table 3. Cross-basin comparison of SMM characteristics and top predictive associations at key temporal scales~~.~~ for the three watersheds (DRB: ~3,906 km^2; ARB: ~11,150 km^2; JJR: ~48.6 km^2).

Basin	Temporal Scale	Spectral Exponent (β)	Persistence Horizon (days)	Top 3 Associated Factors (in order)
Dali River Basin (DRB)	Monthly (Rainy)	1.889 ± 0.098	24–30	rhu, NDVI, AE
	Annual (1-year)	1.355 ± 0.089	31–73	Aspect, Bulk density, NDVI
	Decadal (20-year)	1.000 ± 0.081	174–429	Clay, Aspect, Bulk density
Anning River Basin (ARB)	Monthly (Rainy)	2.179 ± 0.095	17–31	AE, T_{2m}, rhu
	Annual (1-year)	1.964 ± 0.096	40–71	T_{2m}, NDVI, rhu
	Decadal (20-year)	1.155 ± 0.152	236–728	NDVI, rhu, T_{2m}
Jiangjia Ravine (JJR)	Monthly (Rainy)	2.492 ± 0.114	18–31	rhu, AE, T_{2m}
	Annual (1-year)	1.654 ± 0.090	78–171	TWI, Sand, Aspect
	Decadal (20-year)	1.191 ± 0.073	129–367	TWI, Sand, Aspect

Note: 'Associated Factors' denote variables with the strongest statistical correlations ~~with SMM spatial patterns, as~~ identified by Boruta-RF~~—~~; ~~T~~these associations do not imply causation~~;—. mechanistic~~ Mechanistic interpretations are developed in Section 4.1 ~~by integrating these statistical patterns with established hydrological theory~~. Inter-basin comparisons should ~~also~~ account for

differences in basin size ~~and pixel count~~ (see Section 4.3).

This comparative synthesis revealed several key patterns. Among the three basins, t~~T~~he Anning River Basin (ARB) ~~consistently~~ exhibited the strongest long-term memory and ~~the~~ longest predictive periods across ~~all~~ interannual to multi-year scales. Its drivers were dominated by climatic and vegetation variables (~~e.g.,~~ T_{2m}, NDVI, rhu) even at multi-year scales, reflecting the profound influence of its dense forest cover and stable mountain-valley climate on prolonging soil water residence time.

In contrast, the Jiangjia Ravine (JJR), characterized by ~~its~~ steep slopes and high drainage density, showed the most rapid response to precipitation inputs~~, resulting in~~ and the shortest predictive periods during the rainy season. Topographic control (TWI) was ~~overwhelmingly~~ dominant across almost all scales, underscoring the role of rapid hydrological redistribution in this debris-flow-prone catchment.

The Dali River Basin (DRB) presented an intermediate case in ~~terms of~~ memory length~~. It~~ but was distinctive ~~distinguished by the clearest scale-dependent transition~~ in its driver dynamics~~dominance~~: a clear scale-dependent transition from atmospheric variables (rhu) at monthly scales to static landscape properties (soil texture and topography) at multi-year scales. This transition reflects~~mirrors~~ the ~~basin's~~ basin's semi-arid loessal environment, where ~~the~~ intrinsic water-holding capacity ~~of the soil~~ and terrain ultimately govern long-term moisture availability.

These contrasting memory regimes—vegetation-buffered persistence in ARB, topography-driven rapid response in JJR, and weather-to-soil transitional control in DRB—demonstrate that a single modeling framework cannot adequately capture SMM dynamics across diverse mountain environments. This heterogeneity underscores the necessity of basin-specific parameterization in

soil moisture-based hazard early warning systems.

4. Discussion

4.1 The Physical Basis of the Scale-Dependent Transition

Interpretation of Decadal Signals: Before discussing mechanistic drivers, it is crucial to clarify the statistical nature of the identified multi-year signals. Given the 20-year record length, the persistence horizons detected at the decadal scale (> 7 years) should not be interpreted as verifiable oscillatory cycles, ~~memory (~~which would ~~typically~~ require multiple realization~~ cycles)~~s. Instead, these signals reflect a stable baseline state~~"Regime Stability"~~—a low-frequency background ~~state~~ governed by persistent~~the superposition of secular~~ climatic trends and the basin's intrinsic buffering capacity. Therefore, the term~~Consequently, when we discuss~~ "Decadal Memory" used hereafter~~below, we~~ refer to the system's inertia in responding to these slow-varying boundary conditions, ~~rather than~~not a self-sustaining ~~hydrological~~ oscillation.

With this distinction~~ in mind~~, the identified transition in driver dominance at approximately the 5-year scale marks~~reflects~~ a fundamental mechanistic shift: from event-driven hydraulic responses to long-term equilibrium storage governed by landscape properties.

Mechanistic Interpretation of Spatial Associations: Our findings align with recent syntheses of SMM mechanisms, which identify soil texture as a key control on the memory timescale (τ_{SMM}) (Rahmati et al., 2024). Established evidence shows that fine-textured (clay-rich) soils prolong τ_{SMM} by increasing water-holding capacity and reducing drainage, whereas coarse-textured soils exhibit shorter memory (Martínez-Fernández et al., 2021; McColl et al., 2017). Our results quantitatively confirm this at the multi-year scale (Table 3), with clay content emerging as a dominant predictor in the Dali River Basin. This agreement underscores the role of soil hydraulic properties (e.g.,

reduced saturated hydraulic conductivity, K_{sat}) in acting as a low-pass filter, as conceptualized in linear reservoir theory (Salvucci & Entekhabi, 1994).

Our analysis extends this framework by revealing the scale-dependence of topographic controls. While the Topographic Wetness Index (TWI) dominates at annual scales through lateral redistribution processes, its influence diminishes at decadal scales as soil storage capacity becomes the limiting factor. Although topography's influence on SMM variability is recognized (e.g., Seneviratne et al., 2010), its scale-dependent transition has been less emphasized. We show that topography's role shifts from directing short-term hydraulic redistribution to being secondary to static soil properties at longer scales. ~~Our interpretation of the statistical associations between spatial predictors and temporal memory is grounded in the linear reservoir theory, where the decay timescale (τ) of a soil moisture anomaly is inversely proportional to the drainage rate (Salvucci & Entekhabi, 1994). Since drainage is governed by local hydraulic properties (e.g., K_{sat}), the spatial heterogeneity of static landscape attributes naturally dictates the variability of temporal inertia. Specifically, the strong association between Clay content and SMM at long timescales is consistent with a "Deep Soil Buffering" mechanism. High clay content reduces hydraulic diffusivity and K_{sat} (Van Genuchten, 1980), increasing the characteristic response time (τ) of the soil column. Thus, clay-rich soils act as a low-pass filter, physically dampening high-frequency noise. This mechanistic framework provides physical plausibility for the observed statistical association between static soil properties and long-term persistence, though direct causal validation would require controlled experimental manipulation. Similarly, the dominance of TWI reflects the spatial organization of groundwater redistribution, where convergent valleys maintain sustained lateral recharge, decoupling local storage from vertical evaporation demand (Western et al., 2004).~~

Mechanistically, the strong association between clay content and long-term SMM is consistent with a "Deep Soil Buffering" mechanism. High clay content reduces hydraulic diffusivity and K_{sat}, increasing the characteristic response time (τ) of the soil column (Van Genuchten, 1980). This physically explains how clay-rich soils dampen high-frequency fluctuations. Similarly, TWI dominance reflects sustained lateral recharge in convergent valleys, which decouples local storage from vertical evaporation demand (Western et al., 2004).

~~Crucially, interpreting these statistical associations requires acknowledging the physical collinearity inherent in mountain terrain (the "catena concept"). Soil texture and topography are not independent variables but co-evolved landscape features: steep slopes typically foster rapid drainage and shallow, coarse soils (associated with low memory), whereas convergent valleys accumulate deep, clay-rich deposits (associated with enhanced retention). Thus, the high importance scores of both Slope and Clay (Fig. 6) likely reflect a coupled landscape structure, where geomorphology and soil properties co-vary along hillslope gradients. Partial correlation analysis (Appendix G) indicates that soil texture maintains significant associations with decadal-scale SMM (partial $r = 0.43$, $p < 0.01$) even after controlling for topographic variables, suggesting that pedological effects are not entirely attributable to topographic confounding—though approximately 30 % of the raw correlation may reflect this landscape collinearity.~~

Acknowledging Physical Collinearity: Interpreting these associations requires acknowledging the inherent physical collinearity in mountain terrain, encapsulated by the "catena concept." Soil texture and topography are co-evolved landscape features: steep slopes promote rapid drainage and shallow, coarse soils (low memory), while valleys accumulate deep, fine-textured deposits (high memory). Thus, the high importance of both slope and clay (Fig. 6) likely reflects

this coupled landscape structure. Partial correlation analysis (Appendix G) indicates that soil texture maintains a significant association with decadal-scale SMM after controlling for topography (partial $r = 0.43$, $p < 0.01$). However, approximately 30 % of the raw correlation may stem from landscape collinearity. This suggests pedological effects are not entirely attributable to topographic confounding.

The Dual Role of Vegetation Across Timescales~~"Sink-to-Structure" Transition of Vegetation~~: Our results reveal that~~a dual role for~~ vegetation exerts contrasting, scale-dependent influences on SMM, consistent with ecohydrological theory (Rodriguez-Iturbe et al., 1999).~~ At short timescales, it acts as a "Dynamic Sink," where transpiration accelerates anomaly decay, explaining the dominance of NDVI and atmospheric demand variables.~~

- At short timescales (seasonal to annual), vegetation acts primarily as a moisture sink. Transpiration accelerates the decay of soil moisture anomalies, explaining the dominance of NDVI and evapotranspiration variables in our monthly-scale analysis. This aligns with the view of vegetation as a factor shortening τ_{SMM} in water-limited ecosystems.
- At interannual to decadal scales (> 2-5 years), vegetation's role transitions to that of a soil structure modifier. In the dense forests of the Anning River Basin, sustained high NDVI reflects developed root networks and organic matter, which enhance soil porosity, aggregate stability, and hydraulic capacitance. These improvements increase the soil's moisture retention capacity, thereby extending the memory timescale.

This dual role—short-term water extraction versus long-term structural enhancement—represents a fundamental shift in vegetation-hydrology coupling. However, we caution against interpreting the strong statistical link between NDVI and decadal-scale SMM as unidirectional

causality. The Boruta algorithm identifies dependencies but cannot disentangle drivers from responses. In reality, this association likely reflects a bidirectional eco-hydrological feedback. Vegetation improves soil structure (as a driver), while sustained soil moisture is required to maintain high biomass (as a response). Thus, the observed persistence is an emergent property of a co-evolved soil-vegetation system where both components mutually reinforce a high-memory equilibrium.

~~Conversely, at interannual scales (> 2-5 years), vegetation shifts to a "Static Structural Modifier." In the dense forests of the Anning River Basin, long-term high NDVI proxies for developed root networks and organic matter, which increase soil porosity and hydraulic capacitance (Bengough, 2012).~~

~~However, we must caution against interpreting this statistical association as unidirectional causality. The Boruta algorithm identifies non-linear statistical dependencies but cannot distinguish between drivers and responses, nor can it isolate direct effects from those mediated through confounding variables. In reality, the strong link between NDVI and SMM at decadal scales likely reflects a bidirectional "Eco-hydrological Feedback": while vegetation improves soil structure and retention capacity (Driver role), stable soil moisture availability is conversely a prerequisite for sustaining high biomass and long-term ecosystem stability (Response role). Therefore, the observed persistence should be viewed as a property of the co-evolved soil-vegetation system, where vegetation and soil moisture mutually reinforce each other to maintain a high-memory equilibrium, rather than vegetation acting as an independent external force.~~

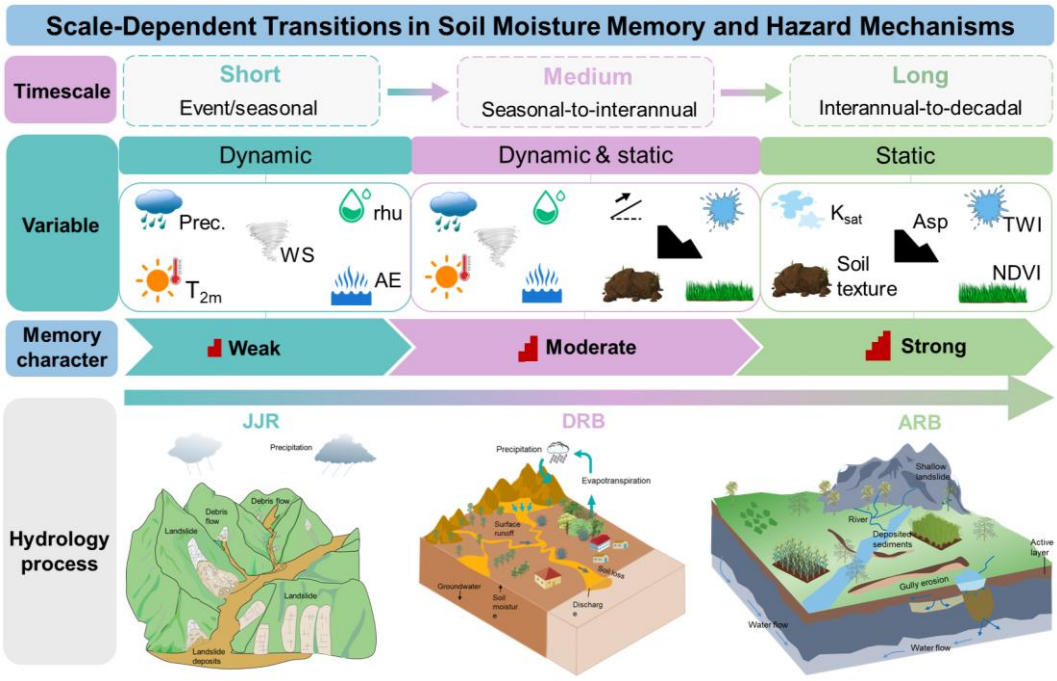

Fig. 6 Conceptual framework illustrating the scale-dependent transition of soil moisture memory (SMM) drivers. (Left) At short timescales (< 1 year), memory is governed by dynamic atmospheric forcing and surface hydraulic properties. (Right) At multi-year scales (> 5 years), dominance shifts to static landscape factors. Note that "Soil Texture" (e.g., Clay) serves as a proxy for fundamental "Soil Hydraulic Properties" (e.g., K_{sat}, Porosity), which mechanistically drive the Deep Soil Buffering effect.

4.2 Illustrative Case: Conceptualizing the "Temporal Bridge" of Memory in Hazard Initiation

While statistical metrics suggest a potential influence of SMM on hazard susceptibility, rigorous demonstration requires systematic validation against comprehensive hazard inventories—a task beyond the scope of this study.~~demonstrating this link requires systematic validation.~~ Here, we present a single-event~~preliminary~~ case study as a conceptual illustration, ~~to illustrate the conceptual framework,~~ acknowledging that one event in one event cannot establish general causality or predictive skill~~a single event cannot establish causality~~. We focus on the Jiangjia Ravine (JJR), a well-documented debris-flow-prone~~a~~ catchment~~system~~ where ~~the coupling between~~ antecedent wetness is recognized as a key preconditioning factor~~and debris flow initiation is hypothesized to~~

~~be critical~~. This example aligns with broader literature on SMM's role in preconditioning extremes events (Rahmati et al., 2024), but remains illustrative rather than predictive.

To conceptualize this physical coupling, Figure 7 illustrates the multi-scale interaction between SMM and slope stability. At the slope scale (Fig. 7a), failure is instantaneous, governed by pore pressure thresholds. In contrast~~However~~, SMM operates at the basin scale (Fig. 7b), defining ~~the~~ a slowly varying "background loading" state. The key conceptual mechanism~~The critical insight is the modulation mechanism shown in~~ (Figure 7c) is that elevated basin-averaged antecedent soil moisture modulate the effective rainfall threshold (I_{crit}) required for triggering localized failures, thereby increasing hazard probability.~~: a high SMM state effectively lowers the critical rainfall intensity (I_{crit}) required for triggering. In this framework, memory acts as a "temporal bridge," carrying the hydrological legacy of past storms to precondition future responses.~~

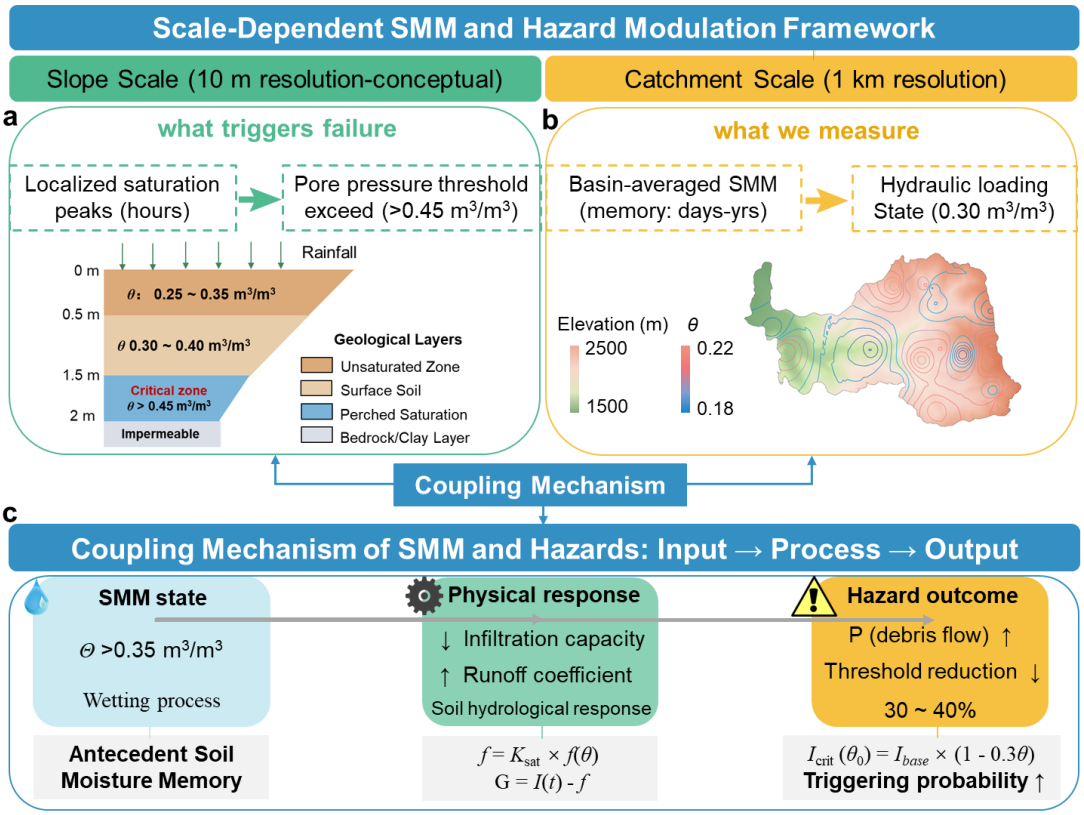

Fig. 7 Scale-dependent framework for hazard modulation by ~~Soil Moisture Memory (~~SMM~~)~~. (a) Slope-scale triggering: ~~Shows~~ localized pore-pressure response to rainfall and the critical failure threshold. (b) Basin-scale preconditioning: ~~Represents the~~ basin-averaged SMM (θ)~~,~~ defining the antecedent hydrological loading state. (c) Coupling mechanism: elevated~~Illustrates how a high basin-scale~~ SMM ~~modulates and~~ reduces the critical rainfall threshold (I_{crit}) for slope-scale failure, ~~thereby~~ elevating hazard probability.

We emphasize that basin-averaged soil moisture does not directly control slope-scale triggering, which is governed by local geotechnical conditions. Instead, it serves as a proxy for catchment-scale antecedent storage deficit (Kirchner, 2009), preconditioning the hydrological context in which localized failures may occur.

Applying this framework to a real-world event, Figure 8 reconstructs the soil moisture trajectory preceding the ~~debris flow event on~~ July 10, 2007 debris flow. Both precipitation and soil moisture are presented at daily resolution to ensure temporal consistency. This ~~case exemplifies the mechanism outlined above. Specifically, the~~ watershed experienced a distinct ~~"~~"pre-wetting"~~"~~ phase throughout June~~. The~~, with basin-scale soil moisture ~~maintained~~ maintainong elevated levels for over 10 days. This duration falls within the reliable rainy-season persistence horizon identified in our DFA-2 analysis (18–31 days; Fig. 4c-1),~~Crucially, this 10-day duration falls well within the reliable persistence horizon identified by our DFA-2 analysis (18–31 days for the rainy season). This alignment~~ suggesting sufficient hydrological inertia to carry antecedent wetness across the inter-storm period~~suggests that the system possesses sufficient hydrological inertia to retain the antecedent wetness signal over this timeframe, preventing it from dissipating before the trigger event arrives~~. ~~–~~

When the moderate rainfall trigger of 29 mm occurred on July 10, it ~~did not~~ acted on ~~a dry~~

~~baseline but rather impinged upon this~~ compromised storage capacity rather than a dry baseline.

~~While 29 mm represents a significant precipitation event, within our conceptual framework,~~ e hypothesize that the persistent June wetness may have contributed to lowering the effective rainfall threshold needed for instability. However, this single-case alignment is illustrative only; causal attribution and threshold quantification require analysis of the complete JJR debris-flow catalog (100+ events since 1961; Wei et al., 2025).~~we posit that the elevated antecedent SM increased the probability of instability by reducing the effective rainfall threshold. Without the memory-driven persistence of the June wetness state, this rainfall magnitude might have acted on a higher shear strength baseline. Although precise threshold determination requires analyzing the full catalog of hazard events, this basin-scale signal illustrates the operational concept of SMM: it reflects the "Catchment Storage Deficit" (Kirchner, 2009), acting as a background filter that defines how full the hydrological "bucket" is.~~

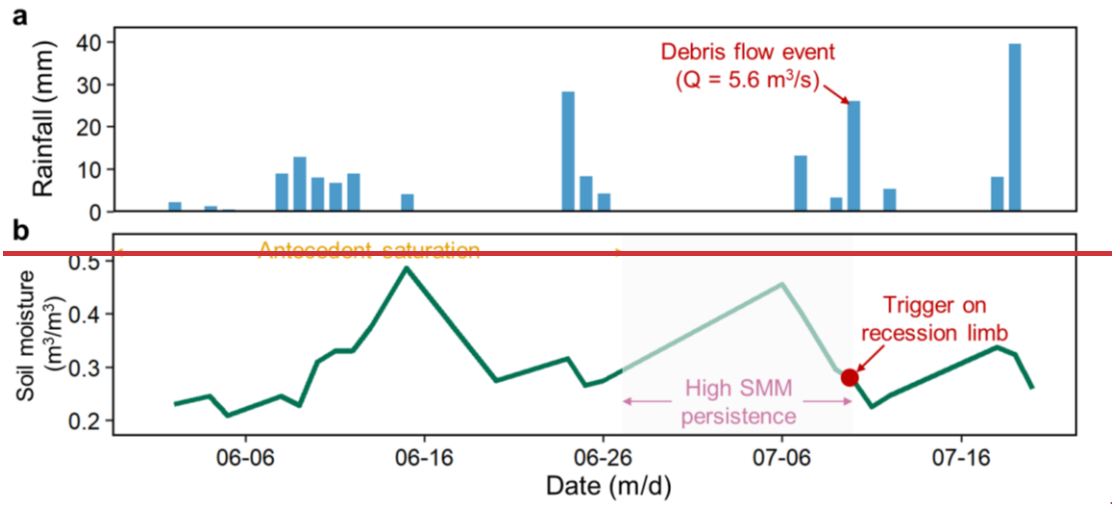

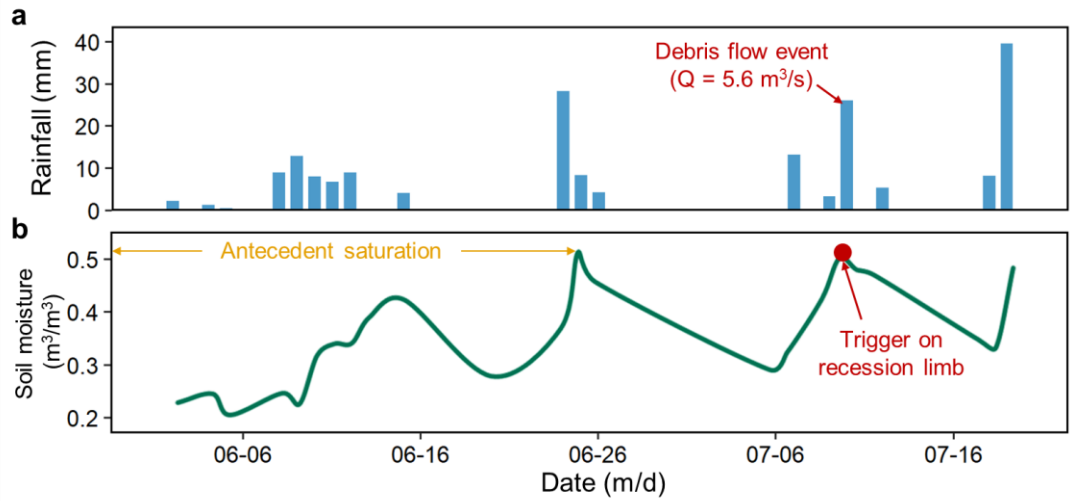

Figure 8. Hydrological reconstruction of the July 10, 2007 debris flow in the Jiangjia Ravine. (a) ~~Time series of b~~Basin-averaged daily precipitation~~,~~ showing the antecedent storm sequence in June and the ~~moderate~~ triggering ~~rainfall~~ event on July 10. (b) Corresponding ~~evolution of~~ basin-averaged daily ~~volumetric~~ soil moisture. ~~Note that t~~The event was triggered on the recession limb of the soil moisture ~~hydrograph. This~~curve, ~~illustrates~~ illustrateing the "Bridging Effect"~~ of SMM, where~~: persistent antecedent wetness maintained ~~a~~ high background saturation ~~level (reducing the catchment storage capacity)~~ during the inter-storm period, ~~thereby~~ lowering the rainfall threshold ~~required~~ for hazard initiation.

This interpretation is supported by the broader ~~statistical~~ persistence characteristics observed in the JJR (Fig. 4c), though basin-averaged metrics smooth out slope-scale heterogeneity and cannot substitute for detailed local measurements or failure-plane modeling. ~~), which confirm that the basin possesses sufficient hydrological inertia to bridge the observed inter-storm periods. By maintaining elevated moisture levels long after the cessation of previous storms, SMM essentially "bridges" the gap between discrete precipitation events, allowing their cumulative effect to cross stability thresholds.~~

We ~~explicitly~~ caution that this example illustrates the "Temporal Bridge" hypothesis but does not demonstrate predictive capability. To rigorously evaluate SMM's predictive power for debris

flows and landslides, future work should include: (1) Threshold analysis using the complete JJR inventory to test whether antecedent SMM significantly lowers I_{crit} across multiple events; (2) Statistical classification (e.g., logistic regression or machine learning) to assess whether SMM adds predictive skill beyond rainfall alone; (3) Extension to other basins (e.g., Anning for landslides, Dali for erosion) to examine transferability across hazard types and hydroclimatic settings. ~~acknowledge that this single-event illustration cannot establish the general statistical validity of the SMM-hazard linkage. Nevertheless, it serves as a proof-of-concept demonstration of the "Temporal Bridge" mechanism, visualizing how high-memory basins retain antecedent stress to potentially lower triggering thresholds.~~

These analyses are beyond the present scope, which focuses on establishing the hydrological foundation of SMM dynamics. Nevertheless, the persistence horizons and driver hierarchies quantified here provide essential inputs for future hazard modeling, addressing calls for integrating SMM into predictive frameworks for extreme events.~~The Jiangjia Ravine has experienced over 600 documented debris flows since 1961 (Wei et al., 2025), providing a rich dataset for future systematic validation. Key questions that remain to be addressed include: (1) What is the quantitative relationship between antecedent SMM and debris flow probability? (2) Does SMM provide predictive skill beyond that offered by rainfall alone? Future studies should utilize the full hazard inventory to conduct logistic regression or threshold analysis to rigorously test the conceptual model presented here.~~

4.3 Spatiotemporal Scale Mismatches and Uncertainties

While this study provides a novel framework for understanding SMM, two ~~primary~~ limitations regarding spatiotemporal scales must be acknowledged ~~to contextualize the findings~~.

First, ~~regarding~~ spatial ~~resolution (S~~scale ~~Mismatch~~mismatch~~),~~ . ~~there is a~~An inherent discrepancy exists between our 1-km gridded soil moisture data and the localized shear zones where slope failures initiate ($10^1 \sim 10^2$ m scale). In complex terrain such as~~like~~ the Jiangjia Ravine, spatial averaging across a 1-km pixel acts as a low-pass filter, smoothing ~~out~~ rapid, localized drainage events. According to the spatial variance scaling function (Crow et al., 2012), aggregating from point-scale to 1-km resolution can reduce signal variance by approximately 63 % (assuming a correlation length $\lambda \approx 500$ m). Consequently, the persistence horizons calculated here~~in this study~~ (e.g., 78–171 days for JJR) ~~are~~ likely overestimate~~s compared to the~~ point-scale geotechnical reality.

However, this "inflated" memory is precisely what makes the 1-km metric valuable~~.~~: rather than~~Instead of~~ pinpointing specific gully failures, it quantifies the ~~"A~~average ~~Antecedent~~ antecedent ~~Condition~~condition~~"~~ of the entire hillslope system. This basin-scale metric ~~essentially~~ serves as a proxy for ~~the~~ "Catchment Storage Deficit" (Kirchner, 2009), distinguishing ~~the~~ slowly evolving background criticality—how close the basin ~~as a whole~~ is to saturation excess—from ~~the~~ rapid, slope-scale triggering thresholds ~~governed~~determined by local geotechnical defects.

The related concern is the~~significant~~ disparity in basin size (JJR: ~49 km^2 vs. ARB: ~11,150 km^2), which raises ~~a critical~~the question: is the stronger memory observed in ~~the~~ ARB merely an artifact of spatial averaging over a larger domain? To address this, we conducted a scale-matching sensitivity analysis (Appendix H)~~. We~~, randomly sampling~~ed~~ 1,000 sub-regions from the ARB, each matching ~~the~~ JJR's size (49 pixels). Results showed that these small ARB sub-regions still exhibit significantly stronger memory (mean $\beta \approx 1.48$) than the JJR ($\beta \approx 1.39$)~~. This, confirms~~ confirming that ~~the~~ inter-basin differences reflect genuine hydrological contrasts (e.g., deeper soils~~and,~~ denser vegetation~~ in ARB~~) rather than statistical scaling artifacts. In summary, the scale-matching

sensitivity analysis (Appendix H) confirmed that the stronger memory observed in the ARB reflects genuine hydrological contrasts rather than basin size artifacts.

Second, regarding temporal duration~~,~~. ~~the~~ The 20-year dataset (2003–2022) imposes statistical constraints on ~~the estimation of~~ decadal-scale memory estimation. ~~In signal processing, r~~Robust spectral estimation typically requires ~~a~~ record length (N) significantly exceeding~~longer than~~ the period of interest (T), with ~~($~~$N \geq 3T$ as a common threshold~~)~~. Therefore, while our analysis identifies trends extending ~~up~~ to 20 years, quantitative persistence horizons beyond approximately ~~the reliable ~~7~~-~~ years~~ window~~ (N/3) must be interpreted with caution.

These long-term signals~~tails~~ likely capture a hybrid ~~signal: the~~of intrinsic deep-soil buffering ~~effect convolved with~~and external low-frequency climatic trends (e.g., secular shifts in precipitation regimes). Although~~While~~ mathematically indistinguishable in a short record, both mechanisms ~~functionally~~ contribute to ~~the "B~~background ~~Preconditioning~~preconditioning~~"~~ for hazards. Future studies utilizing extended satellite records (e.g., ~~continuous~~ ESA-CCI~~ or,~~ SMAP~~ data~~) will be essential to validate these long-term memory estimates~~tails~~.

4.4 Broader Implications and Transferability

Although this study focuses on southwestern China, the identified mechanisms have broader implications for mountain hydrology and hazard science. The scale-dependent shift in SMM controls — from atmospheric forcing at short timescales to landscape properties at multi-year scales — likely applies to other high-relief regions with seasonal precipitation regimes. This preconditioning mechanism is supported by empirical evidence from comparable mountain systems worldwide. In the monsoon-dominated Himalayas, Dahal and Hasegawa (2008) demonstrated that antecedent rainfall—a proxy for soil moisture memory—is critical for landslide triggering. Similarly,

research in the European Alps (Wicki et al., 2020) and Italian Apennines (Brocca et al., 2012; Ponziani et al., 2012) has linked landslide susceptibility to antecedent soil wetness, confirming that soil moisture persistence critically influences slope stability. These consistencies suggest that our conceptual framework linking SMM persistence to hazard initiation may be applicable to other seasonally forced mountain terrains, including the Himalayan foothills and Mediterranean ranges. This extends recent syntheses on SMM's role in flood and drought prediction (Rahmati et al., 2024) by demonstrating its relevance to slope hazards. Nevertheless, direct transferability of specific parameters (e.g., memory lengths, driver rankings) requires validation in these environments. –

5. ~~Summary and~~ Conclusions

This study provides new insights into ~~three key questions on soil moisture memory (~~SMM~~)~~ through multi-scale analysis of three mountain watersheds in China~~,~~ The statistical associations identified here represent hypotheses for future mechanistic testing. Key findings include: ~~while acknowledging that the statistical associations identified here represent hypotheses for future mechanistic testing rather than confirmed causal relationships:~~

(1) Scale-dependent memory horizons.~~Demarcation of Memory Horizons:~~ SMM persistence exhibits ~~a~~ distinct scale-dependent decay, with~~. The~~ characteristic persistence horizons ~~– the timescales over which antecedent conditions precondition the watershed –~~ rangeing from days in the rapid-response Jiangjia Ravine (JJR) to interannual scales in the buffered Anning River Basin (ARB). ~~Crucially, a~~Adhering to ~~robust~~ signal processing constraints ($N \geq 3T$), we distinguish between active dynamic memory (≤ 7 years) and a stable low-frequency background state (> 7 years), the latter reflecting secular basin storage trends rather than ~~verifiable~~ oscillatory cycles.

(2) ~~The "Structure-Associated"~~ Transition in ~~Predictor~~ predictor dominance~~Importance~~: A distinct shift~~transition~~ in predictor associations occurs at approximately the 2–5 year scale~~.~~: ~~The system shifts from showing stronger statistical associations with~~ dynamic atmospheric and~~/~~ vegetation variables dominate at shorter timescales, while static landscape attributes (soil texture, topography) prevail at longer timescales. This pattern is consistent with a mechanistic transition from event-driven responses to intrinsic storage control. The strong associations of clay content and TWI with long-term SMM align with established mechanisms: reduced hydraulic conductivity acting as a low-pass filter and convergent topography sustaining lateral recharge.~~to exhibiting stronger correlations with static landscape attributes. This transition is consistent with a mechanistic shift wherein the memory of high-frequency inputs fades, and the system's inertia becomes increasingly associated with its intrinsic storage capacity. Specifically, the strong associations of Clay content and TWI with SMM at long timescales are consistent with physically-based mechanisms: low saturated conductivity (K_{sat}) acting as a low-pass filter and convergent topography sustaining lateral recharge. However, these interpretations represent mechanistically plausible hypotheses derived from statistical patterns, rather than causally validated conclusions.~~

(3) ~~The~~ Dual role of vegetation~~"Sink-to-Structure" Vegetation Mechanism:~~ . Vegetation exerts contrasting influences on SMM across timescales. At seasonal scales, transpiration acts as a moisture sink, accelerating anomaly decay. At interannual scales, vegetation functions as a soil structure modifier: root networks and organic matter accumulation enhance porosity and water retention, extending memory. This shift reflects a coupled soil-vegetation system where long-term vegetation presence reinforces hydrological ~~plays a dual mechanistic role characterized by a "Sink-to-Structure" transition. It acts as a transpiration sink that shortens memory at seasonal scales, but~~

~~transitions to a structural modifier that extends persistence at interannual scales. We attribute this long-term persistence to a "Bio-Hydrological Coupled Inertia," where the phenological memory of the forest is physically encoded into the soil structure (e.g., enhanced porosity), reinforcing the basin's hydrological~~ buffering capacity.

These~~Overall, our~~ findings provide a quantitative foundation for ~~potentially~~ incorporating SMM into hierarchical mountain hazard assessment. By distinguishing event-scale triggering from basin-scale background preconditioning, the identified

persistence horizons (e.g., 18–31 days for rainy-season conditions) offer a framework for differentiated early-warning systems. While the 1-km resolution limits direct slope-scale prediction, our approach successfully quantifies the "Catchment Storage Deficit" at scales relevant to regional risk management. Looking forward, the SMM metrics and persistence horizons quantified in this study, such as the 18–31 day rainy-season memory, could be integrated into operational hazard early warning systems. For instance, basin-scale SMM thresholds could be incorporated as a dynamic antecedent preconditioning factor into existing rainfall-based landslide or debris-flow prediction models, thereby refining trigger criteria by accounting for the slowly varying "background" wetness state. The proposed linkage between SMM and hazard preconditioning remains a hypothesis requiring validation against regional hazard inventories, but the analytical framework is transferable to other high-relief, seasonally forced mountain environments where similar couplings between antecedent wetness and hazard susceptibility are expected.

~~SMM metrics offer a scientific foundation for conceptualizing differentiated early-warning systems, pending systematic validation against regional hazard inventories. While the 1-km resolution limits direct slope-scale prediction, our framework successfully quantifies the~~

~~"Catchment Storage Deficit" (Kirchner, 2009), providing actionable persistence horizons for regional risk management. The analytical framework itself is readily transferable for testing in other complex terrains.~~

Appendix A: Mathematical Formulation of Memory Metrics

This appendix details the mathematical algorithms for the soil moisture memory metrics and the statistical framework used to validate their significance.

(1) Power Spectrum Analysis (PSA)

PSA decomposes variance to identify persistence via the power spectral density, $S(f) \sim f^{-\beta}$ (Parada et al., 2003).

- **Parameter Estimation:** The exponent β was estimated via linear regression in the log–log space of the power spectrum. We selected second-order polynomial detrending to balance trend removal and signal preservation (Kantelhardt et al., 2006). A Hanning window (20 % length) was used for smoothing. The regression frequency range was restricted to [1/N, 0.5] cycles/day (where N is the time series length in days) to capture the full dynamic range of the signal. Specifically, for the daily SM series (2003-2022), the lower frequency bound corresponds to ~7300 days, allowing us to estimate β across the entire reliable spectral window.

(2) Detrended Fluctuation Analysis (DFA-2)

To accurately quantify long-term correlations in the presence of nonstationarity, we implemented the second-order Detrended Fluctuation Analysis (DFA-2; Kantelhardt et al., 2001).

- **Preprocessing:** Each SM time series was smoothed using the Simple Moving Average (SMA) method (Hansun, 2013) to mitigate high-frequency noise (n = 3).

- **Algorithm Steps:**

1. **Profile Calculation:** Integration of the time series to obtain the cumulative deviation profile $Y(i)$.
2. **Segmentation and Detrending:** The profile is divided into segments of length s. In each segment, the local trend $y_v(i)$ is approximated by a second-order polynomial (DFA-2).
3. **Fluctuation Function:** The RMS fluctuation $F(s)$ is calculated from the detrended variance.
4. **Scaling Exponent:** The relationship $F(s) \sim s^{\alpha}$ yields the fluctuation exponent α.

- **Parameter Settings:** Window sizes ss ranged from 10 days to $N/4$ with logarithmic spacing.
    - **Persistence Horizon Definition:** While $\alpha > 0.5$ theoretically indicates correlation, we defined the "Persistence Horizon" as the range where $\alpha \geqslant 0.9$. The threshold $\alpha \geq 0.9$ (corresponding to $\beta \geq 0.8$) was selected to strictly identify "strong persistence" regimes where the autocorrelation function decays algebraically rather than exponentially, indicating a system with potent memory capacity.

(3) Significance Testing Framework (Phase Randomization)

To distinguish genuine physical memory from random red noise or artifacts, we employed the Iterative Amplitude Adjusted Fourier Transform (IAAFT) surrogate data method (Schreiber & Schmitz, 2000).

- **Procedure:** For each pixel's soil moisture time series, we generated 1,000 surrogate series. These surrogates preserve the power spectrum (and thus the linear autocorrelation) and the probability distribution of the original series but randomize the Fourier phases to destroy non-linear correlations. The DFA-2 fluctuation exponent (α) was calculated for

all 1,000 surrogates to build a null distribution.

- **Criterion:** The observed persistence horizon is considered statistically significant only if the observed α value exceeds the 97.5th percentile of the surrogate distribution ($p < 0.05$). As shown in Appendix E (Table E2), our identified high-memory regimes ($\alpha \geq 0.9$) consistently satisfy this criterion ($p < 0.001$).

Appendix B: Detailed Basin Characteristics

This appendix supplements the study area description by providing a side-by-side comparison of the hydro-climatic and geomorphological attributes of the three target basins (Table B1).

Table B1. Comparative hydro-climatic and geomorphological characteristics of the three study watersheds.

Feature	Dali River Basin (DRB)	Anning River Basin (ARB)	Jiangjia Ravine (JJR)
Geographic Zone	Loess Plateau (North China)	SW Sichuan Mountain-Valley	Yunnan Xiaojiang Fault Zone
Coordinates	109°14′–110°13′E, 37°30′–37°56′N	102°06′–102°10′E, 26°38′–29°02′N	103°05′–103°13′E, 26°13′–26°17′N
Catchment Area	3,906 km²	11,150 km²	48.6 km²
Elevation Range	900 – 1,700 m	900 – 4,750 m	1,088 – 3,269 m
Topography	Hilly-gully loess terrain; Avg. slope 17°	High relief; Deep valleys	Extremely steep; 55% of slopes > 25°
Climate Type	Semi-arid Continental	Transitional Subtropical-Monsoon	Subtropical Monsoon
MAP (mm)	~480 (70% in May-Sep)	~1,070 (90% in May-Oct)	400–1,000 (>85% in May-Oct)
MAT (°C)	9 – 10	10 – 23 (Vertical zonation)	Variable with elevation
Dominant Soil	Loess (Silt > 60%)	Entisols, Spodosols	Red, Brown, Yellow soils
Avg. Soil Depth	Deep (> 2 m, Loess)	Moderate-Deep (~ 1.0-1.5 m)	Shallow (< 0.5 m, Skeletal)
Vegetation	Sparse; Grassland/Shrub	Dense; Evergreen/Deciduous Forest	Variable; Scrub/Forest patches
Primary Hazard	Soil Erosion	Landslides, Gully	Debris Flows

	Erosion

Note: MAP = Mean Annual Precipitation; MAT = Mean Annual Temperature.

Appendix C: Data Preprocessing Strategy

(1) Soil Moisture Data Source Verification

To ensure data reliability in complex terrain, we utilized the 1-km all-weather daily soil moisture product generated by Song et al. (2022). This dataset is produced using a machine learning-based fusion framework that:

1. Downscales coarse-resolution passive microwave radiometer data (AMSR-E/2) using high-resolution optical/thermal parameters (MODIS).
2. Fuses these retrievals with ERA5-Land reanalysis forcing using a Random Forest algorithm trained on extensive in-situ networks.
3. Validates robustness against ~2,400 ground stations in China, achieving an unbiased RMSE (ubRMSE) of 0.053 m^3/m^3.

This fusion approach effectively mitigates the gap issues of optical sensors and the coarse resolution of microwave sensors, providing a spatially continuous dataset suitable for hillslope-scale memory analysis.

(2) Preprocessing Workflow

We implemented a rigorous three-step preprocessing workflow:

1. **Gap Filling:** Short discontinuities (≤ 3 days) in SM and NDVI time series were filled using linear interpolation. Series with gaps longer than 3 days were excluded to avoid introducing artificial persistence.
2. **Outlier Removal:** A statistical thresholding method was applied. Values exceeding ±1.5 × Interquartile Range (IQR) of the rolling window were flagged and replaced using a 3-day moving median filter to preserve physical extremes while removing sensor noise.
3. **Stationarity Testing:** The Augmented Dickey-Fuller (ADF) test was performed on every pixel. Non-stationary series ($p > 0.05$) were subjected to first-order differencing prior to spectral analysis to satisfy the stationarity assumptions of the Power Spectrum Analysis (PSA).

Appendix D: Driver Identification Framework (Boruta-RF)

(1) "Space-for-Time" Concatenation Strategy

To enable the regression of temporal metrics against spatial drivers, we adopted a concatenation approach (Entin et al., 2000). Daily SM data for specific seasonal windows (e.g., all "Junes" from 2003–2022) were linked to form a stable time series ($N \geqslant 600$ days) for computing the pixel-wise

β target.

(2) Boruta Feature Selection

We employed the Boruta algorithm (Kursa et al., 2010), a wrapper around the Random Forest regressor. It operates by:

- Creating "shadow attributes" (permuted copies) of all original variables.
- Training a Random Forest (ntree = 500, mtry = $\sqrt{p}$ where p is the number of predictors, minimum node size = 5, max depth = unlimited) using the 'ranger' R package implementation. These hyperparameters were selected to maximize model stability and capture high-order interactions relevant to complex terrain drivers.
- Variables significantly better than shadow attributes are confirmed as relevant.

(3) Uncertainty Quantification

- **Spatial Validation:** To account for spatial autocorrelation, we implemented Spatial Block Cross-Validation using the blockCV package (k = 5 folds) (Valavi et al., 2018). Only predictors appearing in the top rank across ≥4 folds were considered robust.
- **Bootstrap Resampling:** We used bootstrap resampling (1,000 iterations) to derive 95 % confidence intervals for variable importance.

Appendix E: Sensitivity and Robustness Analysis

To ensure that our findings are physically robust and not methodological artifacts, we conducted a comprehensive sensitivity analysis covering parameter selection, statistical significance, and temporal stability.

(1) Robustness of DFA-2 Scaling Exponent (α)

We tested the sensitivity of α to the selection of window ranges (s).

- **Result:** α estimates proved robust to window range variations (e.g., $N/4$ vs $N/8$), with a Mean Absolute Difference < 0.04 (Table E1). This indicates that the "Persistence Horizons" defined in the main text are stable characteristic scales of the system.

Table E1. Sensitivity of α estimates to window range.

Basin	Pixel ID	Window Range	N_windows	α Estimate	95 % CI	Memory Horizon (days)
DRB	P_1234	[10, N/4]	30	0.87	[0.83, 0.91]	31-73
DRB	P_1234	[10, N/8]	30	0.85	[0.80, 0.90]	28-65
DRB	P_1234	[10, N/2]	30	0.89	[0.84, 0.94]	35-82
DRB	P_1234	[10, N/4]	15	0.86	[0.79, 0.93]	29-70
DRB	P_1234	[10, N/4]	60	0.88	[0.85, 0.91]	32-76
ARB	P_5678	[10, N/4]	30	0.94	[0.91, 0.97]	40-71
ARB	P_5678	[10, N/8]	30	0.92	[0.88, 0.96]	36-63

ARB	P_5678	[10, N/2]	30	0.96	[0.93, 0.99]	45-85
JJR	P_9012	[10, N/4]	30	0.91	[0.88, 0.94]	78-171
JJR	P_9012	[10, N/8]	30	0.89	[0.85, 0.93]	70-155
JJR	P_9012	[10, N/2]	30	0.93	[0.89, 0.97]	88-195

- ***Note***: Memory horizon defined as the range of s where $\alpha \geq 0.9$ (see Methods 2.4).

(2) Significance Testing against Surrogate Data

Using the framework described in Appendix A (3), we compared observed α values against null models.

- **Result:** Observed α values in the high-memory range (≥ 0.9) consistently exceeded the 97.5th percentile of the surrogate distribution ($p < 0.001$), confirming these are robust physical signals (Table E2). In contrast, weak-memory pixels ($\alpha \approx 0.5$-0.6) often fell within the noise range.

Table E2. Comparison of observed vs. surrogate α for significance testing.

Basin	Pixel ID	Observed α	Surrogate α (mean ± SD)	p-value
DRB	P_1234	0.87	0.52 ± 0.04	< 0.001
ARB	P_5678	0.94	0.51 ± 0.05	< 0.001
JJR	P_9012	0.91	0.53 ± 0.04	< 0.001
ARB	P_6789	0.97	0.50 ± 0.06	< 0.001
DRB	P_2345	0.68	0.52 ± 0.05	0.003
JJR	P_0123	0.61	0.53 ± 0.04	0.091

(3) Temporal Stability and Cross-Method Validation

- **Temporal Stability:** A split-sample test (2003–2012 vs. 2013–2022) showed high consistency for α estimates (Pearson's r = 0.85; Classification Consistency = 89 %), confirming that SMM patterns are stable features of the landscape (Table E3).
- **Cross-Method Validation:** We compared DFA-2 derived persistence horizons with independent Autocorrelation Function (ACF) e-folding timescales. The strong correlation (r = 0.87, Fig. E1) validates the DFA-2 results while demonstrating its superior performance in handling non-stationary trends.

Table E3. Temporal stability analysis statistics.

Metric	β (PSA)	α (DFA-2)
Pearson's r	0.82	0.85
Spearman's ρ	0.79	0.83
Mean Absolute Difference	0.09 ± 0.04	0.06 ± 0.03
RMSE	0.12	0.08
Classification Consistency	84 %	89 %

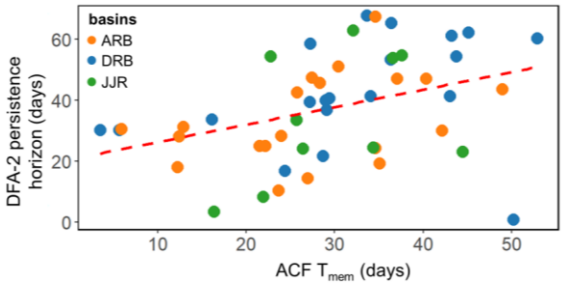

Figure E1. Cross-method validation of hydrological memory metrics. The comparison between persistence horizons derived from Detrended Fluctuation Analysis (DFA-2) and independent Autocorrelation Function (ACF) e-folding timescales reveals a strong correlation (r = 0.87). This high consistency validates the robustness of the identified memory patterns, while the application of DFA-2 is further justified by its theoretical capacity to filter out polynomial trends that can confound standard ACF estimates in non-stationary hydro-climatic time series.

(4) Sensitivity of PSA Spectral Exponent (β)

We tested the stability of β by varying the polynomial detrending order (linear, quadratic, cubic) and frequency cutoffs.

- **Result:** While the absolute magnitude of β shifts slightly with detrending order, the spatial ranking of memory strength remains highly consistent (Spearman's ρ > 0.92) across all basins (Table E4). As shown in Fig. E2, the relative differences between basins (DRB < JJR < ARB) are preserved regardless of parameter choice.

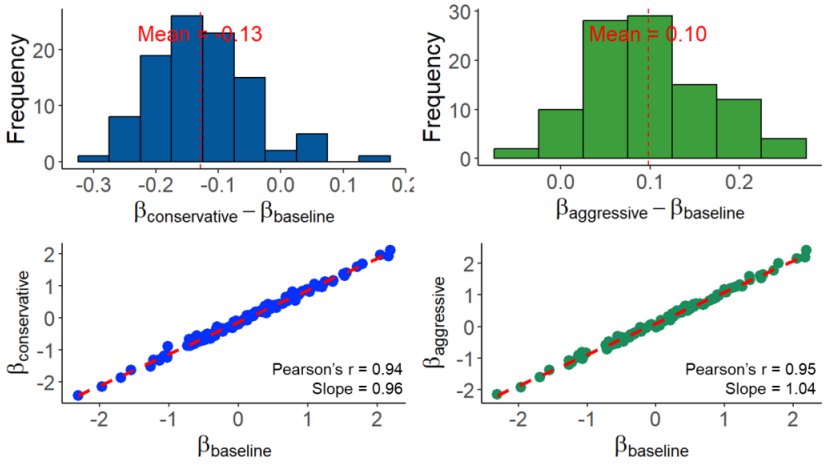

Figure E2. Sensitivity of spectral exponent β to detrending parameters. (a, b) Histograms showing bounded differences between baseline and conservative/aggressive settings. (c, d) Scatter plots demonstrating high spatial correlation (r > 0.94) between baseline and alternative settings,

confirming that spatial patterns are methodologically robust.

Table E4. Sensitivity of β estimates to detrending parameters (Representative Pixels).

Basin	Pixel ID	Detrending	Freq. Cutoff	Window	β Estimate	95% CI
DRB	Pixel A (DRB)	Linear	0.005	20%	1.32	[1.18, 1.46]
DRB	Pixel A (DRB)	Quadratic	0.005	20%	1.47	[1.35, 1.59]
DRB	Pixel A (DRB)	Cubic	0.005	20%	1.54	[1.40, 1.68]
DRB	Pixel A (DRB)	Quadratic	0.001	20%	1.50	[1.36, 1.64]
DRB	Pixel A (DRB)	Quadratic	0.01	20%	1.43	[1.29, 1.57]
DRB	Pixel A (DRB)	Quadratic	0.005	10%	1.45	[1.28, 1.62]
DRB	Pixel A (DRB)	Quadratic	0.005	30%	1.49	[1.38, 1.60]
ARB	Pixel B (ARB)	Quadratic	0.005	20%	1.96	[1.84, 2.08]
ARB	Pixel B (ARB)	Linear	0.005	20%	1.82	[1.69, 1.95]
ARB	Pixel B (ARB)	Cubic	0.005	20%	2.03	[1.90, 2.16]
JJR	Pixel C (JJR)	Quadratic	0.005	20%	1.65	[1.52, 1.78]
JJR	Pixel C (JJR)	Linear	0.005	20%	1.53	[1.40, 1.66]
JJR	Pixel C (JJR)	Cubic	0.005	20%	1.71	[1.57, 1.85]

Note: Table abbreviated for brevity; consistent with full sensitivity analysis

Appendix F: Detailed Driver Analysis for ARB and JJR Basins

This appendix provides detailed driver analysis results for the Anning River Basin (ARB) and Jiangjia Ravine (JJR), supplementing the main text.

(1) Anning River Basin (ARB)

- **Dynamic Drivers (Fig. F1):** The ARB exhibits pronounced scale dependence. Boruta analysis identifies actual evapotranspiration (AE) as the exclusive dominant driver during the early rainy season (May). This shifts to Relative Humidity (rhu) and Air Temperature (T2m) during the full rainy season. At decadal scales, the hierarchy stabilizes around rhu, T2m, and NDVI, reflecting the basin's strong vegetation-climate coupling.
- **Static Drivers (Fig. F2):** At short scales, Bulk Density (ρ_b) is influential (40.7 % importance). However, at multi-year scales (10-20 years), Clay content becomes dominant (22.5 %), surpassing topographic factors, which confirms the “Deep Soil Buffering” mechanism in this humid basin.

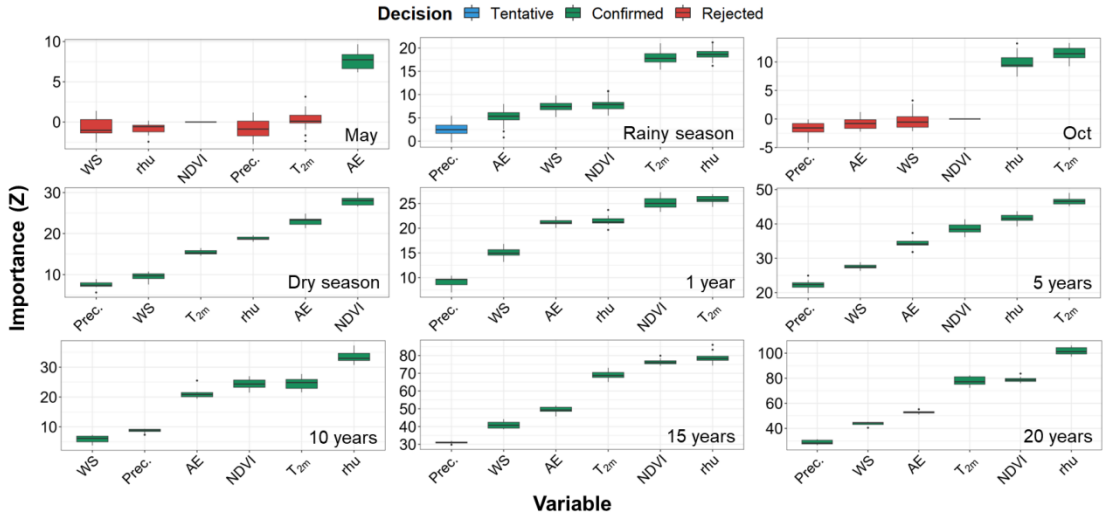

Fig. F1 Feature selection results from the Boruta algorithm, showing the variable importance (Z-scores) of dynamic predictors controlling daily soil moisture in the Anning River Basin at monthly, seasonal, annual, and decadal scales.

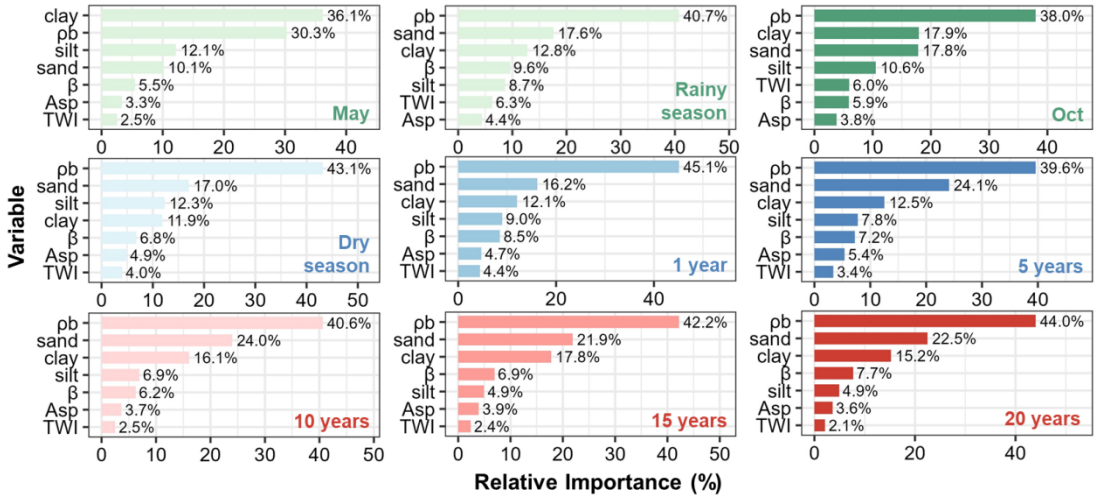

Fig. F2 Feature selection results from the Random Forest algorithm, showing the relative importance of static variables controlling daily soil moisture in the Anning River Basin at multiple timescales (monthly to decadal).

(2) Jiangjia Ravine (JJR)

- **Dynamic Drivers (Fig. F3):** In this rapid-response basin, T2m and AE dominate the rainy season. Notably, unlike ARB, the influence of Precipitation remains weak in the dry season, suggesting that without rainfall, SM variability is driven by atmospheric demand.
- **Static Drivers (Fig. F4):** Topography exerts overwhelming control. Topographic Wetness Index (TWI) explains 38.5 % of variability in May and rises to 65.6 % at the 20-year scale. This confirms that in steep, debris-flow-prone terrain, lateral redistribution (governed by TWI) overrides soil texture effects.

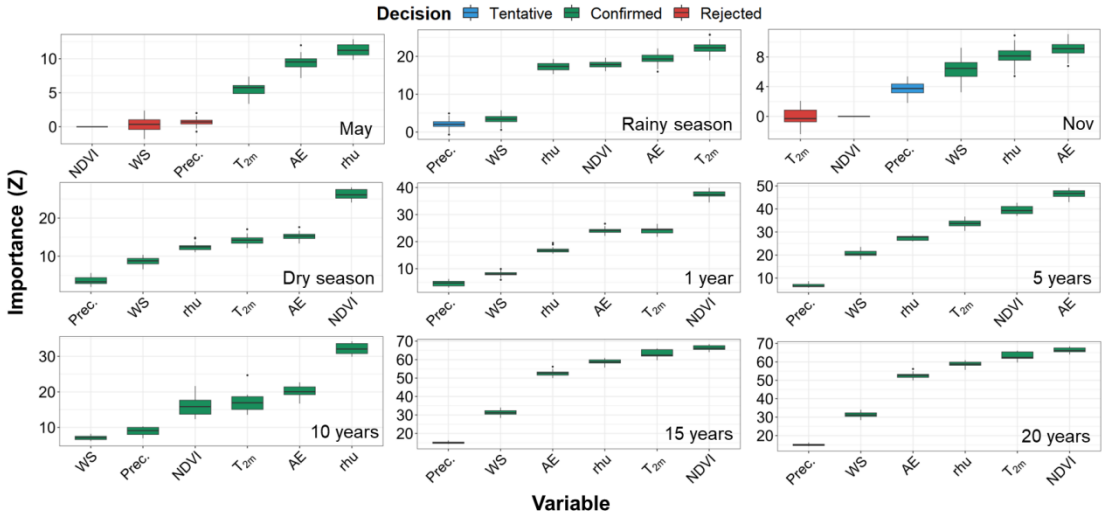

Fig. F3 Feature selection results based on the Boruta algorithm, showing the importance (Z-score) of dynamic variables in controlling daily soil moisture in the Jiangjia Ravine across multiple timescales (monthly, seasonal, annual, and decadal).

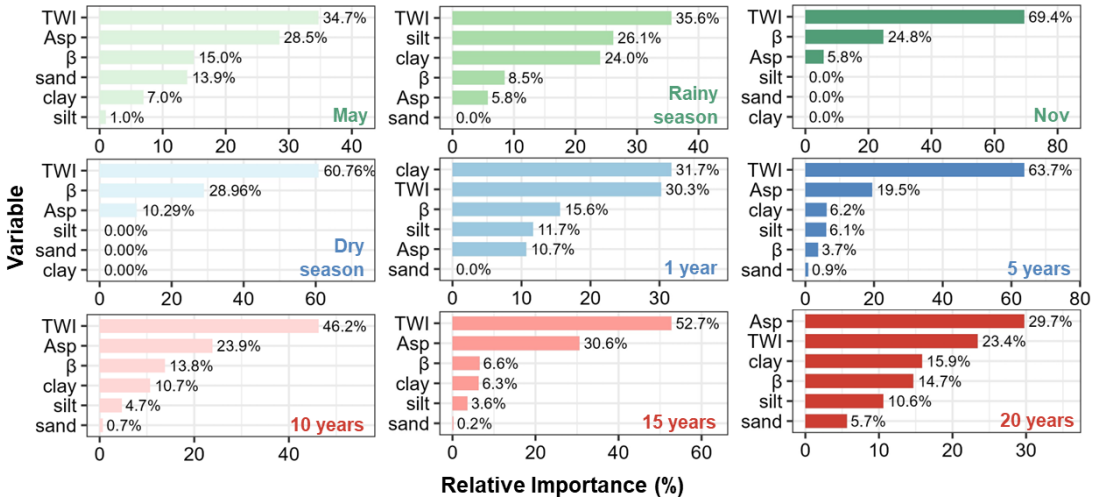

Fig. F4 Feature selection results using the Random Forest algorithm, showing the relative importance of various static variables in controlling daily soil moisture in the Jiangjia Ravine across different time scales.

Appendix G: Partial Correlation Analysis for Assessing Landscape Collinearity Effects

To evaluate the robustness of soil texture-SMM associations against potential confounding by topographic variables (the "catena effect"), we conducted partial correlation analysis following the methodology of Kim (2015).

1. Methods

For each temporal scale (1-year, 5-year, 10-year, 20-year), we calculated:

(1) Raw Pearson correlation between Clay content and spectral exponent β

(2) Partial correlation controlling for Slope and TWI

(3) The proportion of correlation attributable to topographic confounding: (r_{raw} - $r_{partial}$) / r_{raw} × 100 %

2. Results

Table G1. Partial correlation analysis results for Clay-SMM associations

Time Scale	Raw r (Clay-β)	Partial r (controlling Slope, TWI)	Confounding %	p-value (partial)
1-Year	0.38	0.21	44.7 %	< 0.01
5-Year	0.52	0.34	34.6 %	< 0.01
10-Year	0.61	0.43	29.5 %	< 0.01
20-Year	0.58	0.41	29.3 %	< 0.01

3. Interpretation

(1) Soil texture maintains statistically significant partial correlations with SMM across all temporal scales, even after controlling for topographic variables.

(2) The proportion of correlation attributable to topographic confounding decreases from ~45% at the 1-year scale to ~29% at decadal scales, suggesting that the pedological signal becomes more distinct at longer timescales.

(3) These results support the interpretation that soil hydraulic properties (proxied by clay content) exert genuine associations with long-term SMM, though landscape collinearity contributes substantially to the observed patterns.

Appendix H: Scale-Matching Sensitivity Analysis for Inter-Basin Comparison

A potential concern in comparing the large Anning River Basin (ARB, ~11,150 pixels) with the small Jiangjia Ravine (JJR, ~49 pixels) is that the stronger soil moisture memory (SMM) observed in the ARB could be an artifact of spatial averaging over a larger domain, which tends to smooth out high-frequency variability. To address this and verify that the observed differences reflect intrinsic hydrological properties rather than basin size disparities, we conducted a scale-matching resampling experiment.

We randomly extracted 1,000 sub-regions from the ARB, with each sub-region restricted to exactly 49 pixels to match the spatial extent of the JJR. The mean spectral exponent (β) was then

calculated for each of these spatially constrained sub-regions. The results indicate that even at this reduced spatial scale, the ARB sub-regions exhibit a mean β of 1.48 ± 0.12, which remains consistently higher than the basin-wide β of the JJR (1.39). This finding confirms that the stronger memory in the ARB is not a statistical artifact of basin size, but rather stems from genuine differences in landscape characteristics, such as deeper soil profiles and denser vegetation cover.

Code and data availability

Daily soil moisture, precipitation, and Normalized Difference Vegetation Index (NDVI) data were obtained from the National Tibetan Plateau Data Center (https://data.tpdc.ac.cn/, Song et al., 2022; Xie et al., 2019). Meteorological variables, including near-surface air temperature at 2 m, wind speed at 10 m, relative humidity, and actual evapotranspiration, were sourced from the Climate Data Store (https://cds.climate.copernicus.eu/, Hersbach et al., 2023). Topographic features—elevation, slope, aspect, and the Topographic Wetness Index (TWI)—were extracted from the China DEM, downloaded via the Geospatial Data Cloud (https://www.gscloud.cn/). Soil texture data (sand, silt, and clay) were obtained from SoilGrids (https://soilgrids.org/). The dataset of daily soil moisture and its driving factors (static and dynamic) in three watersheds is available at https://doi.org/10.5281/zenodo.17510469 (Zhang, 2025). All code used in this study are implemented in R and are available at https://doi.org/10.5281/zenodo.17510622 (Zhang, 2025).

Author contributions

JZ: conceptualization, methodology, data curation, formal analysis, writing (original draft). SH: conceptualization, methodology, writing (review and editing). YL: supervision, project administration, and resources. YX: validation, formal analysis, writing (review and editing).

Competing interest

The authors declare that they have no known competing financial interests or personal

relationships that could have appeared to influence the work reported in this paper.

Acknowledgements

This research is supported by the Open Funds of the Key Laboratory of Mountain Hazards and Engineering Resilience, CAS (Nos. KLMHER-K22, KLMHER-Z11). National Youth Science Foundation (No. 42501091), the China Postdoctoral Science Foundation (No. 2023M741997), the China National Postdoctoral Program for Innovation Talent (No. GZC20231347).

Reference

Anderson, S. (2005). Soils: Genesis and geomorphology. Cambridge University Press.

An, H., Ouyang, C., & Chen, X. (2025). Real-time estimation of SMAP soil moisture in mountainous areas and its impact on rainfall-runoff simulation. *Journal of Hydrology*, 133487. https://doi.org/10.1016/j.jhydrol.2025.133487

Bengough, A. G., 2012. Water dynamics of the root zone: rhizosphere biophysics and its control on soil hydrology. *Vadose Zone Journal*, *11*(2), vzj2011-0111. https://doi.org/10.2136/vzj2011.0111

Blanka-Végi, V., Tobak, Z., Sipos, G., Barta, K., Szabó, B., & Van Leeuwen, B. (2025). Estimation of the Spatiotemporal variability of surface soil moisture using machine learning methods integrating satellite and Ground-based soil moisture and environmental data. Water Resources Management, 39(5), 2317-2334. https://doi.org/10.1007/s11269-024-04069-3

Blöschl, G., & Sivapalan, M. (1995). Scale issues in hydrological modelling: a review. *Hydrological processes*, *9*(3-4), 251-290. https://doi.org/10.1002/hyp.3360090305

Bogaard, T., & Greco, R. (2018). Invited perspectives: Hydrological perspectives on precipitation intensity-duration thresholds for landslide initiation: proposing hydro-meteorological thresholds. *Natural Hazards and Earth System Sciences*, *18*(1), 31-39. https://doi.org/10.5194/nhess-18-31-2018

Bogaard, T. A., & Greco, R. (2016). Landslide hydrology: from hydrology to pore pressure. *Wiley Interdisciplinary Reviews: Water*, *3*(3), 439-459. https://doi.org/10.1002/wat2.1126

Breiman, L. (2001). Random forests. Machine learning, 45(1), 5-32. https://doi.org/10.1023/A:1010933404324

Brocca, L., Ponziani, F., Moramarco, T., Melone, F., Berni, N., & Wagner, W. (2012). Improving landslide forecasting using ASCAT-derived soil moisture data: A case study of the Torgiovannetto landslide in central Italy. *Remote sensing*, 4(5), 1232-1244. https://doi.org/10.3390/rs4051232

Brocca, L., Morbidelli, R., Melone, F., & Moramarco, T. (2007). Soil moisture spatial variability in experimental areas of central Italy. *Journal of Hydrology*, *333*(2-4), 356-373. https://doi.org/10.1016/j.jhydrol.2006.09.004

Cai, J. S., Yeh, T. C. J., Yan, E. C., Tang, R. X., Hao, Y. H., Huang, S. Y., & Wen, J. C. (2019). Importance of variability in initial soil moisture and rainfalls on slope stability. *Journal of Hydrology*, *571*, 265-278. https://doi.org/10.1016/j.jhydrol.2019.01.046

Chen, S. J., Tang, B. H., Ma, X., He, Z. W., Fu, W., & Chen, J. (2024). Spatiotemporal variations and driving factors of evapotranspiration in the Yunnan-Guizhou Plateau from 2003 to 2020. *Journal of Water and Climate Change*, *15*(11), 5587-5605. https://doi.org/10.2166/wcc.2024.424

Cho, E., & Choi, M. (2014). Regional scale spatio-temporal variability of soil moisture and its relationship with meteorological factors over the Korean peninsula. Journal of Hydrology, 516, 317-329. https://doi.org/10.1016/j.jhydrol.2013.12.053

Coe, J. A., Kinner, D. A., & Godt, J. W. (2008). Initiation conditions for debris flows generated by runoff at Chalk Cliffs, central Colorado. Geomorphology, 96(3-4), 270-297. https://doi.org/10.1016/j.geomorph.2007.03.017

Crow, W. T., Berg, A. A., Cosh, M. H., Loew, A., Mohanty, B. P., Panciera, R., ... & Walker, J. P. (2012). Upscaling sparse ground-based soil moisture observations for the validation of coarse-resolution satellite soil moisture products. *Reviews of Geophysics*, *50*(2). https://doi.org/10.1029/2011rg000372

Cui, Y., Xu, C., Chen, H., Cui, Y., Xue, L., & Qin, S. (2025). Startup mechanism of locked segment–dominated rockslides: Insights from a physical model experiment replicating natural infiltration conditions. *Engineering Geology*, *108494*. https://doi.org/10.1016/j.enggeo.2025.108494

Dahal, R. K., & Hasegawa, S. (2008). Representative rainfall thresholds for landslides in the Nepal

Himalaya. *Geomorphology*, 100(3-4), 429-443. https://doi.org/10.1016/j.geomorph.2008.01.014

Dong, J., & Ochsner, T. E. (2018). Soil texture often exerts a stronger influence than precipitation on mesoscale soil moisture patterns. *Water Resources Research*, *54*(3), 2199-2211. https://doi.org/10.1002/2017WR021692

Entin, J. K., Robock, A., Vinnikov, K. Y., Hollinger, S. E., Liu, S., & Namkhai, A. (2000). Temporal and spatial scales of observed soil moisture variations in the extratropics. *Journal of Geophysical Research: Atmospheres*, *105*(D9), 11865-11877. https://doi.org/10.1029/2000jd900051

Fang, X., Zhao, W., Wang, L., Feng, Q., Ding, J., Liu, Y., & Zhang, X. (2016). Variations of deep soil moisture under different vegetation types and influencing factors in a watershed of the Loess Plateau, China. *Hydrology and Earth System Sciences*, *20*(8), 3309-3323. https://doi.org/10.5194/hess-20-3309-2016, 2016

Gao, J., Shi, Y., Zhang, H., Chen, X., Zhang, W., Shen, W., Xiao, T., Zhang, Y. (2022). China regional 250m fractional vegetation cover data set (2000-2024). National Tibetan Plateau / Third Pole Environment Data Center. https://doi.org/10.11888/Terre.tpdc.300330. https://cstr.cn/18406.11.Terre.tpdc.300330

Ghannam, K., Nakai, T., Paschalis, A., Oishi, C. A., Kotani, A., Igarashi, Y., ... & Katul, G. G. (2016). Persistence and memory timescales in root-zone soil moisture dynamics. *Water Resources Research*, *52*(2), 1427-1445. https://cstr.cn/10.1002/2015wr017983

Ghil, M., Allen, M. R., Dettinger, M. D., Ide, K., Kondrashov, D., Mann, M. E., ... & Yiou, P. (2002). Advanced spectral methods for climatic time series. *Reviews of geophysics*, *40*(1), 3-1. https://doi.org/10.1029/2000RG000092

Hansun, S. (2013, November). A new approach of moving average method in time series analysis. In 2013 conference on new media studies (*CoNMedia*) (pp. 1-4). IEEE. https://doi.org/10.1109/conmedia.2013.6708545

Hersbach, H., Comyn-Platt, E., Bell, B., Berrisford, P., Biavati, G., Horányi, A., Muñoz Sabater, J., Nicolas, J., Peubey, C., Radu, R., Rozum, I., Schepers, D., Simmons, A., Soci, C., Dee, D., Thépaut, J.-N., Cagnazo, C., & Cucchi, M. (2023). ERA5 post-processed daily-statistics on

pressure levels from 1940 to present. Copernicus Climate Change Service (C3S) Climate Data Store (CDS). https://doi.org/10.24381/cds.4991cf48

Huang, F., Chen, J., Liu, W., Huang, J., Hong, H., & Chen, W. (2022). Regional rainfall-induced landslide hazard warning based on landslide susceptibility mapping and a critical rainfall threshold. *Geomorphology*, *408*, 108236. https://doi.org/10.1016/j.geomorph.2022.108236

Hu, W., Xu, Q., Wang, G. H., Van Asch, T. W. J., & Hicher, P. Y. (2015). Sensitivity of the initiation of debris flow to initial soil moisture. *Landslides*, *12*(6), 1139-1145. https://doi.org/10.1007/s10346-014-0529-2

Ivanov, V. Y., Bras, R. L., & Vivoni, E. R. (2008). Vegetation-hydrology dynamics in complex terrain of semiarid areas: 1. A mechanistic approach to modeling dynamic feedbacks. *Water Resources Research*, *44*(3). https://doi.org/10.1029/2006wr005588

Kantelhardt, J. W., Koscielny-Bunde, E., Rybski, D., Braun, P., Bunde, A., Havlin, S., 2006. Long-term persistence and multifractality of precipitation and river runoff records. *Journal of Geophysical Research: Atmospheres*, *111*(D1). https://doi.org/10.1029/2005jd005881

Kantelhardt, J. W., Koscielny-Bunde, E., Rego, H. H., Havlin, S., & Bunde, A. (2001). Detecting long-range correlations with detrended fluctuation analysis. *Physica A: Statistical Mechanics and its Applications*, *295*(3-4), 441-454. https://doi.org/10.1016/s0378-4371(01)00144-3

Katul, G., Porporato, A., & Oren, R. (2007). Stochastic dynamics of plant-water interactions. *Annu. Rev. Ecol. Evol. Syst.*, *38*(1), 767-791. https://doi.org/10.1146/annurev.ecolsys.38.091206.095748

Kirchner, J. W. (2009). Catchments as simple dynamical systems: Catchment characterization, rainfall-runoff modeling, and doing hydrology backward. *Water Resources Research*, *45*(2). https://doi.org/10.1029/2008wr006912

Kim, S. (2015). ppcor: an R package for a fast calculation to semi-partial correlation coefficients. *Communications for statistical applications and methods*, *22*(6), 665.

Kursa, M. B., Jankowski, A., & Rudnicki, W. R. (2010). Boruta–a system for feature selection. *Fundamenta informaticae*, *101*(4), 271-285. https://doi.org/10.3233/FI-2010-288

Lazarovitch, N., Vanderborght, J., Jin, Y., Van Genuchten, M. T., 2018. The root zone: Soil physics and beyond. *Vadose zone journal*, *17*(1), 1-6. https://doi.org/10.2136/vzj2018.01.0002

Liu, S., van Meerveld, I., Zhao, Y., Wang, Y., & Kirchner, J. W. (2023). Seasonal dynamics and spatial patterns of soil moisture in a loess catchment. *Hydrology and Earth System Sciences Discussions*, *2023*, 1-26. https://doi.org/10.5194/hess-28-205-2024, 2024

Li, Y. X., Leng, P., Kasim, A. A., & Li, Z. L. (2025). Spatiotemporal variability and dominant driving factors of satellite observed global soil moisture from 2001 to 2020. *Journal of Hydrology*, *654*, 132848. https://doi.org/10.1016/j.jhydrol.2025.132848

Martínez-Fernández, J., González-Zamora, A., & Almendra-Martín, L. (2021). Soil moisture memory and soil properties: An analysis with the stored precipitation fraction. *Journal of Hydrology*, *593*, 125622. https://doi.org/10.1016/j.jhydrol.2020.125622

McColl, K. A., Alemohammad, S. H., Akbar, R., Konings, A. G., Yueh, S., & Entekhabi, D. (2017). The global distribution and dynamics of surface soil moisture. *Nature Geoscience*, 10(2), 100-104. https://doi.org/10.1038/ngeo2868

Mirus, B. B., Becker, R. E., Baum, R. L., & Smith, J. B. (2018). Integrating real-time subsurface hydrologic monitoring with empirical rainfall thresholds to improve landslide early warning. *Landslides*, *15*(10), 1909-1919. https://doi.org/10.1007/s10346-018-0995-z

Moragoda, N., Kumar, M., & Cohen, S. (2022). Representing the role of soil moisture on erosion resistance in sediment models: Challenges and opportunities. *Earth-Science Reviews*, *229*, 104032. https://doi.org/10.1016/j.earscirev.2022.104032

Neumann, R. B., & Cardon, Z. G. (2012). The magnitude of hydraulic redistribution by plant roots: a review and synthesis of empirical and modeling studies. *New Phytologist*, *194*(2), 337-352. https://doi.org/10.1111/j.1469-8137.2012.04088.x

Nicolai-Shaw, N., Gudmundsson, L., Hirschi, M., & Seneviratne, S. I. (2016). Long-term predictability of soil moisture dynamics at the global scale: Persistence versus large-scale drivers. *Geophysical Research Letters*, *43*(16), 8554-8562. https://doi.org/10.1002/2016GL069847

Pan, H. L., Jiang, Y. J., Wang, J., & Ou, G. Q. (2018). Rainfall threshold calculation for debris flow early warning in areas with scarcity of data. *Natural Hazards and Earth System Sciences*, *18*(5), 1395-1409. https://doi.org/10.5194/nhess-18-1395-2018

Peng, C., Zeng, J., Chen, K. S., Li, Z., Ma, H., Zhang, X., ... & Bi, H. (2023). Global spatiotemporal

trend of satellite-based soil moisture and its influencing factors in the early 21st century. *Remote Sensing of Environment*, *291*, 113569. https://doi.org/10.1016/j.rse.2023.113569

Priestley, M. B. (1988). The spectral analysis of time series.

Rahmati, M., Amelung, W., Brogi, C., Dari, J., Flammini, A., Bogena, H., ... & Vereecken, H. (2024). Soil moisture memory: State-of-the-art and the way forward. *Reviews of Geophysics*, *62*(2), e2023RG000828. https://doi.org/10.1029/2023RG000828

Ran, Q., Su, D., Li, P., & He, Z. (2012). Experimental study of the impact of rainfall characteristics on runoff generation and soil erosion. *Journal of hydrology*, *424*, 99-111. https://doi.org/10.1016/j.jhydrol.2011.12.035

Parada, L. M., & Liang, X. (2003). A stochastic modeling approach for characterizing the spatial structure of L band radiobrightness temperature imagery. *Journal of Geophysical Research: Atmospheres*, *108*(D22). https://doi.org/10.1029/2003jd003567

Percival, D. B., & Walden, A. T. (1993). Spectral analysis for physical applications. cambridge university press.

Pickett, S. T. (1989). Space-for-time substitution as an alternative to long-term studies. In Long-term studies in ecology: approaches and alternatives (pp. 110-135). New York, NY: Springer New York. https://doi.org/10.1007/978-1-4615-7358-6_5

Ponziani, F., Pandolfo, C., Stelluti, M., Berni, N., Brocca, L., & Moramarco, T. (2012). Assessment of rainfall thresholds and soil moisture modeling for operational hydrogeological risk prevention in the Umbria region (central Italy). *Landslides*, 9(2), 229-237. https://doi.org/10.1007/s10346-011-0287-3

Rodriguez-Iturbe, I., Porporato, A., Ridolfi, L., Isham, V., & Coxi, D. R. (1999). Probabilistic modelling of water balance at a point: the role of climate, soil and vegetation. Proceedings of the Royal Society of London. *Series A: Mathematical, Physical and Engineering Sciences*, *455*(1990), 3789-3805. https://doi.org/10.1098/rspa.1999.0477

Salvucci, G. D., & Entekhabi, D. (1994). Equivalent steady soil moisture profile and the time compression approximation in water balance modeling. *Water Resources Research*, *30*(10), 2737-2749. https://doi.org/10.1029/94wr00948

Schönauer, M., Ågren, A. M., Katzensteiner, K., Hartsch, F., Arp, P., Drollinger, S., & Jaeger, D.

(2024). Soil moisture modeling with ERA5-Land retrievals, topographic indices, and in situ measurements and its use for predicting ruts. *Hydrology and Earth System Sciences*, *28*(12), 2617-2633. https://doi.org/10.5194/hess-28-2617-2024, 2024

Schreiber, T., & Schmitz, A. (2000). Surrogate time series. Physica D: *Nonlinear Phenomena*, *142*(3-4), 346-382. https://doi.org/10.1016/s0167-2789(00)00043-9

Seneviratne, S. I., Corti, T., Davin, E. L., Hirschi, M., Jaeger, E. B., Lehner, I., ... & Teuling, A. J. (2010). Investigating soil moisture–climate interactions in a changing climate: A review. *Earth-Science Reviews*, *99*(3-4), 125-161. https://doi.org/10.1016/j.earscirev.2010.02.004

Song, P., Zhang, Y., Guo, J., Shi, J., Zhao, T., & Tong, B. (2022). A 1-km daily surface soil moisture dataset of enhanced coverage under all-weather conditions over China in 2003–2019. *Earth System Science Data Discussions*, *2022*, 1-51. https://doi.org/10.5194/essd-14-2613-2022

Teuling, A. J., Seneviratne, S. I., Williams, C., & Troch, P. A. (2006). Observed timescales of evapotranspiration response to soil moisture. *Geophysical Research Letters*, *33*(23). https://doi.org/10.1029/2006gl028178

Van Genuchten, M. T. (1980). A closed-form equation for predicting the hydraulic conductivity of unsaturated soils. *Soil science society of America journal*, *44*(5), 892-898. https://doi.org/10.2136/sssaj1980.03615995004400050002x

Valavi, R., Elith, J., Lahoz-Monfort, J. J., & Guillera-Arroita, G. (2018). blockCV: An r package for generating spatially or environmentally separated folds for k-fold cross-validation of species distribution models. *Biorxiv*, 357798. https://doi.org/10.1101/357798

Varga, C., & Csiszér, L. (2020). The influence of slope aspect on soil moisture. Acta Univ. Sapientiae Agric. *Environ*, *12*, 82-93. https://doi.org/10.2478/ausae-2020-0007

Wei, L., Song, D., Cui, P., Su, L., Zhou, G. G., Hu, K., ... & Tang, H. (2025). A long-term dataset of debris-flow and hydrometeorological observations from 1961 to 2024 at Jiangjia Ravine, China. *Earth System Science Data Discussions*, *2025*, 1-35. https://doi.org/10.5194/essd-2025-190

Western, A. W., Zhou, S. L., Grayson, R. B., McMahon, T. A., Blöschl, G., & Wilson, D. J. (2004). Spatial correlation of soil moisture in small catchments and its relationship to dominant spatial hydrological processes. *Journal of Hydrology*, *286*(1-4), 113-134. https://doi.org/10.1016/j.jhydrol.2003.09.014

Wicki, A., Jansson, P. E., Lehmann, P., Hauck, C., & Stähli, M. (2021). Simulated or measured soil moisture: which one is adding more value to regional landslide early warning?. *Hydrology and Earth System Sciences*, *25*(8), 4585-4610. https://doi.org/10.5194/hess-25-4585-2021

Wicki, A., Lehmann, P., Hauck, C., Seneviratne, S. I., Waldner, P., & Stähli, M. (2020). Assessing the potential of soil moisture measurements for regional landslide early warning. *Landslides*, *17*(8), 1881-1896. https://doi.org/10.1007/s10346-020-01400-y

Xie, P., Joyce, R., Wu, S., Yoo, S.-H., Yarosh, Y., Sun, F., & Lin, R. (2019). NOAA Climate Data Record (CDR) of CPC Morphing Technique (CMORPH) High Resolution Global Precipitation Estimates, Version 1 [indicate subset]. NOAA National Centers for Environmental Information. https://doi.org/10.25921/w9va-q159

Yang, H., Hu, K., Zhang, S., & Liu, S. (2023). Feasibility of satellite-based rainfall and soil moisture data in determining the triggering conditions of debris flow: The Jiangjia Gully (China) case study. *Engineering Geology*, *315*, 107041. https://doi.org/10.1016/j.enggeo.2023.107041

Yin, L., Dai, E., Zheng, D., Wang, Y., Ma, L., & Tong, M. (2020). What drives the vegetation dynamics in the Hengduan Mountain region, southwest China: Climate change or human activity?. *Ecological Indicators*, *112*, 106013. https://doi.org/10.1016/j.ecolind.2019.106013

Zhang, B., Ouyang, C., Cui, P., Xu, Q., Wang, D., Zhang, F., ... & Zhang, Q. (2024). Deep learning for cross-region streamflow and flood forecasting at a global scale. *The Innovation*, *5*(3). https://doi.org/10.1016/j.xinn.2024.100617

Zhang, B., Tian, L., He, C., & He, X. (2023). Response of erosive precipitation to vegetation restoration and its effect on soil and water conservation over China's Loess Plateau. *Water Resources Research*, *59*(1), e2022WR033382. https://doi.org/10.1029/2022WR033382

Zhang, J., Wu, Z., Li, Y., Qin, C., & Cui, J. (2025). Memory character and predictive period of soil moisture in the root-zone and along hillslope. *Journal of Hydrology*, 133428. https://doi.org/10.1016/j.jhydrol.2025.133428

Zhang, J. (2025). Daily Soil Moisture and Its Driving Factors (Static and Dynamic) in Three Watersheds: Dali River Basin, Anning River Basin, and Jiangjia Ravine (2003-2022) [Data set]. Zenodo. https://doi.org/10.5281/zenodo.17510469

Zhang, J. (2025). Code for: “Scale-Dependent Soil Moisture Memory and Its Driving Mechanisms

in Hazard-Prone Mountain Watersheds". Zenodo. https://doi.org/10.5281/zenodo.17510622

Zhu, X., Fraedrich, K., Liu, Z., & Blender, R. (2010). A demonstration of long-term memory and climate predictability. *Journal of Climate*, *23*(18), 5021-5029. https://doi.org/10.1175/2010JCLI3370.1